Hindawi
Advances in Civil Engineering
Volume 2020, Article ID 1046937, 25 pages
https://doi.org/10.1155/2020/1046937

Research Article

Design of Groundwater Extraction in Open Cut Foundation Pit and Simplified Calculation of Ground Subsidence due to Dewatering in Sandy Pebble Soil Strata

Lu Zhang,[1,2] **Xiaojun Zhou**,[1] **Yingdong Pan**,[1] **Bowen Zeng**,[1] **Dongfeng Zhu**,[3] **and Huaizu Jiang**[3]

[1]*Key Laboratory of Transportation Tunnel Engineering of Ministry of Education, School of Civil Engineering, Southwest Jiaotong University, Chengdu 610031, China*
[2]*China Railway First Survey and Design Institute Group Co., Ltd, Bridge and Tunnel Design Office, Xi'an 710043, China*
[3]*Rail Transit Construction Corp. Ltd. of the 21st China Railway Construction Corporation Ltd., Jinan 250021, China*

Correspondence should be addressed to Xiaojun Zhou; zhouxjyu69@163.com

Received 22 August 2019; Revised 22 December 2019; Accepted 23 December 2019; Published 27 January 2020

Academic Editor: Rafael J. Bergillos

In order to study the design of incomplete well point for groundwater extraction in open cut foundation pit in which the inner and outer aquifers are not completely isolated and the change mechanism of ground subsidence due to dewatering in the foundation pit, an open cut foundation pit for a subway station on Chengdu Metro Line 6 is taken as an example; meanwhile, the typical sandy pebble soil strata are also considered as a research object in this paper. Firstly, a new method for designing groundwater extraction in the open cut foundation pit is presented and applied to the practical project. The dewatering funnel curve is derived based on Dupuit's assumption, and the ground subsidence around the foundation pit due to groundwater extraction is calculated using the stratification summation method as well as considering the effect of seepage force. The finite difference software FLAC^{3D} is employed to simulate the groundwater extraction process in the foundation pit, and the simulation of groundwater extraction by single well point and group well points is also carried out and the unapparent effect of group well points is obtained. The comparison among on-site monitoring, theoretical calculation, and numerical simulation shows that these values have the same trend in indicating ground subsidence, and the conventional stratification summation method is conservative, and the algorithm considering the effect of seepage force is more accurate. Therefore, the ground subsidence curve caused by groundwater extraction in the foundation pit is presented. The above research methods and results can be applicable for practical engineering and be used to guide the design and construction of groundwater extraction in the foundation pit by using the open cut method in sandy pebble soil strata.

1. Introduction

With the rapid development of economy, the construction of cities is remarkably increasing, and the urbanization process is being apparently accelerated, so more and more urban underground spaces are being exploited in cities around the world. Thus, urban high-rise buildings and underground municipal facilities are being increasingly developed in densely packed urban areas.

Since most city subway stations are being built in bustling area, due to the influence of the narrower construction site and heavier traffic flow, the foundation pit for building a subway station can only be excavated under the condition without ground water. At such narrower and bustling urban area, there is no possibility of performing groundwater extraction outside the open cut foundation pit. Therefore, groundwater extraction inside the foundation pit is usually employed in the design and excavation of foundation pits for building underground subway stations; in addition, a large number of bored waterproof curtains are adopted in consideration of such factors as construction difficulty

and cost. The waterproof curtains refer to the ones that do not penetrate the entire aquifer but enter a certain depth in the aquifer and combine the design of groundwater extraction in the foundation pit to form a groundwater treatment method for internal water lowering and external water stopping. When groundwater extraction inside a foundation pit is carried out, the groundwater outside the pit will bypass the bottom of the waterproof curtains and pass through the aquifer into the foundation pit. Compared with the dewatering outside the foundation pit, it not only increases the seepage path of the foundation pit but also reduces the head loss outside the foundation pit. The influence of dewatering inside the foundation pit on the surrounding environment is less than the one caused by the dewatering outside the pit. If it is a fully enclosed foundation pit, to be specific, the enclosure structure or the diaphragm walls can then be extended to the bottom of the aquifer and be inserted into impermeable stratum underneath the bottom, the groundwater outside the foundation pit will be completely isolated from that one inside the pit. Currently, groundwater extraction in the foundation pit basically has no effect on ground surface outside the foundation pit. If it is a semiclosed foundation pit, that is, the waterproof structure or the diaphragm wall is inserted into the middle and lower parts of the aquifer, the groundwater inside and outside the upper foundation pit will be discontinuous, and the bottom aquifer will become continuous. Therefore, the groundwater inside the foundation pit can be replenished by the aquifer outside the pit. At this time, the groundwater extraction in the foundation pit will lead to a series of problems, such as ground subsidence, deformation of support structure, and uplift of the bottom of the foundation pit. Among them, the ground subsidence outside the pit is more likely to occur, so this paper focuses on addressing the problem.

Yihdego [1] studied the relationship between the reduction in flow and cutoff of hydraulic barriers in a period of time and found the effect of barriers begins to be significant after cutoff exceeds 60%. But as for this project, the inserted depth of enclosure structures is far smaller than the distance between the bottom of the foundation pit and the top of the impermeable layer, so the inserted depth is not considered, and the enclosure structures have no effect on groundwater flow below the foundation pit ideally. And the design scheme of groundwater extraction in the open cut foundation pit is illustrated in Figure 1.

In Figure 1, H indicates the thickness of the phreatic aquifer, e.g., original water table in the foundation pit, m; S denotes the maximal depth of dewatering outside the foundation pit, m; S_w denotes the depth of dewatering in the well point, m; h' indicates the water head at the bottom of the central axis of the enclosure structure, m; and h denotes the water level after dewatering in the foundation pit, m.

Many scholars have studied the dewatering in the foundation pit. Zhang et al. [2] proposed an analytical calculation method for predicting tunnel deformation induced by upside excavation and also discussed the role of dewatering in the deformation mechanism. Wang et al. [3] established a conceptual and mathematical model that considered hydrogeological conditions, curtain depth, and pumping well screens and performed numerical simulations based on the model. Xu et al. [4] investigated the engineering geology and hydrogeology related to foundation dewatering and discussed the current state of foundation dewatering works resulting in land subsidence in Shanghai. Wang et al. [5] introduced a transparent soil model test to address the limitation of the existing experimental method and numerical simulations in modeling the coupling mechanism between the cutoff wall and the pumping wells and proposed the optimal depth of the pumping wells and the optimal horizontal distance between the cutoff wall and the pumping wells. In order to analyze the influence of layering, the mechanical parameters, and the relationship between ground settlements and drawdown, Pujades et al. [6] adopted a radially symmetric conceptual model and conducted several hydromechanical simulations by varying the boundary conditions, the size of the modeled domain, and the presence or absence of an overlying layer. Based on a large deep excavation of the buildings in Oriental Fisherman's Wharf, Wang et al. [7] performed single-well and group-well field pumping tests and carried out a numerical simulation by using the 3D finite difference method (FDM). Taking Qianjiang Century City Station foundation pit as an example, Wang et al. [8] performed field experiments to observe the coupling non-Darcy flow in round gravel, established a generalized conceptual model to study the coupling effect under different combinations of curtain and pumping wells, and carried out numerical simulations of the coupling non-Darcy flow in foundation pit dewatering based on Forchheimer's equation. Based on a deep excavation project in Tianjin, Wu et al. [9] conducted field measurements of the groundwater head and the building settlement during excavation and analyzed the influence range of dewatering and the relationship between the drawdown head and the settlement. To predict the behavior of land subsidence due to groundwater extraction, Zhang et al. [10] established a three-dimensional numerical model considering the confined aquifer and soft deposit and then analyzed and compared between the calculated result and measured value. This paper mainly takes the dewatering project of an open cut foundation pit of a metro station on Chengdu Metro Line 6 as an example. The results of ground subsidence around the foundation pit calculated by using theoretical formulae and numerical simulation FLAC^{3D} are, respectively, compared with the on-site monitoring data. The design scheme of the foundation pit dewatering is also proposed, and the ground subsidence curve caused by dewatering is also compared. Thus, the results proposed in this paper can be used as a reference and guidance for similar projects under similar geological conditions.

2. Design and Calculation of Dewatering in Foundation Pit

2.1. Calculation of Dewatering in Foundation Pit in Single Soil Layer under Waterproofing Enclosure Structure. It is seen

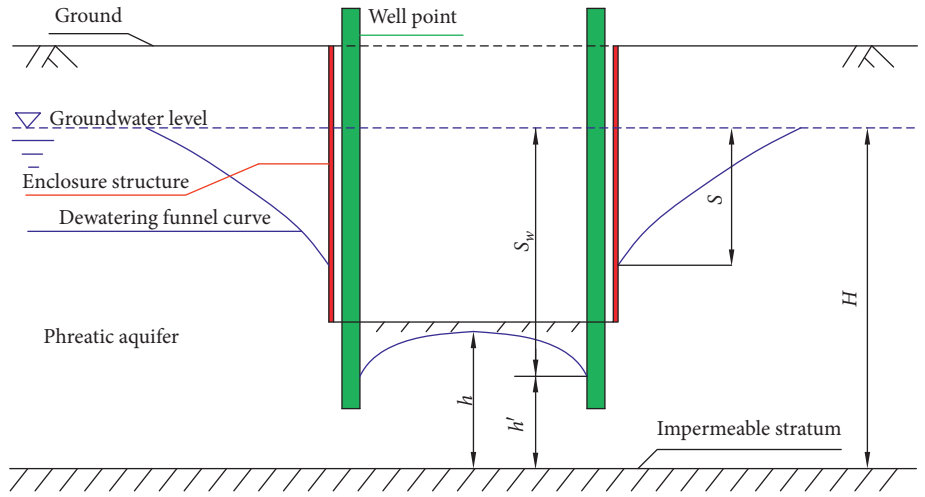

Figure 1: Schematic diagram of dewatering design in the open cut foundation pit.

from references [11–13] that if the boundary of the seepage field is impervious, the flow line in the flow net is parallel to the boundary, and while the seepage field is equal to the water head boundary, the flow line is orthogonal to the seepage boundary. Therefore, the seepage field around the foundation pit under the geological conditions of single-layered soil is shown in Figure 2.

Both the enclosure structure and the bottom impervious layer can be regarded as impervious boundaries, and the horizontal seepage velocity of the groundwater at the bottom of the enclosure structure is far greater than its vertical one, so the flow of groundwater at different depths below the bottom of the center axis of the enclosure structure is approximately regarded as horizontal flow, that is, laminar flow. Therefore, the water head line at the bottom of the central axis of the enclosure structure is vertical. Thus, according to these vertical flow lines, the seepage field around the foundation pit is divided into two seepage fields, respectively, one is inside the foundation pit and the other is outside the foundation pit. Water inflow from the two seepage fields can then be solved separately. It is known that the groundwater outside the pit provides water inflow for groundwater inside the pit; thus, the water inflow Q_1 inside the pit is equal to the water inflow Q_2 outside the pit, namely,

$$Q_1 = Q_2. \tag{1}$$

The radius of influence is defined as the maximum distance at which the drawdowns can be detected with the usual measure devices in the field [14]. The most common way to find the radius of influence is the use of empirical formulae [15–17], such as Sichardt's formula as well as Kusakin's formula. Furthermore, related influence factors like time t and radius of the pit r_e are also taken into account in the formulae by some scholars [15–17]. In this project, the design is based on the Chinese Code. According to the Chinese Technical Specification for Retaining and Protection of Building Foundation Excavations (JGJ 120-2012) [18], the radius of influence for phreatic aquifers in the

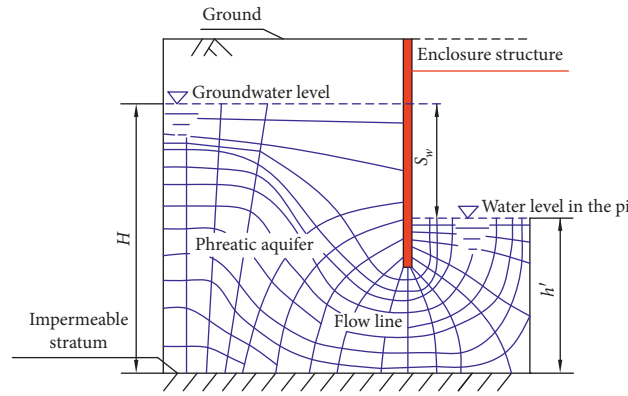

Figure 2: Seepage field distribution around a single-layered soil foundation pit.

foundation pit can be calculated according to the following equation:

$$R = 2S_w\sqrt{Hk}, \tag{2}$$

where R is the radius of influence, m; S_w denotes the depth of dewatering in the well point, m; H indicates the thickness of the phreatic aquifer, e.g., original water table in the foundation pit, m; and k refers to the permeability coefficient of the ground, m/d.

In order to analyze the water inflow inside and outside the foundation pit, two conditions are taken into account as follows:

① If considering the enclosure structure as the wall of a well point, the entire foundation pit can then be considered as a submersible incomplete well, and the water inflow outside the foundation pit away from the boundary can be calculated approximately by using the normative formula presented in the Technical Specification JGJ 120-2012 [18]. As for a circular or a rectangular pit with length-width ratio less than 20, the water inflow Q_2 is calculated according to the following equation [19]:

$$Q_2 = \frac{1.366k\left(H^2 - h_m^2\right)}{\lg\left(1 + \left(R/r_0\right)\right) + \left(\left(h_m - l\right)/l\right)\lg\left(1 + 0.2\left(h_m/r_0\right)\right)}, \tag{3}$$

$$h_m = \frac{H + h'}{2}, \tag{4}$$

where r_0 stands for the equivalent radius of the foundation pit, m; it is calculated according to $r_0 = 0.565\sqrt{A_0}$; A_0 denotes the foundation pit area, m^2; h' indicates the water head at the bottom of the central axis of the enclosure structure, m; and l means the length of the water inlet part of the dewatering well, m.

② The enclosure structure and the bottom boundary are both impervious layers. According to Darcy's seepage experimental conditions, the seepage field distribution in Figure 3 is simplified to be a one-dimensional flow field distribution as shown in Figure 4.

That is, in the assumption that the groundwater in the pit one-dimensionally flows in a circular glass tube and it satisfies Darcy's flow law, water inflow Q_1 into the pit is derived theoretically as follows:

$$Q_1 = \frac{kA\left(h' - h\right)}{L}, \tag{5}$$

$$A = \frac{V}{L}, \tag{6}$$

$$V = \pi r_0^2\left(l_2 + l_3\right), \tag{7}$$

$$L = \frac{\left(2l_2 + l_3 + r_0\right)}{2}, \tag{8}$$

$$H = l_1 + l_2 + l_3, \tag{9}$$

$$h = l_2 + l_3, \tag{10}$$

$$S_w = H - h', \tag{11}$$

where h denotes water head height in the foundation pit after dewatering, m; l_1 denotes water table drawdown in the foundation pit, m; l_2 refers to the distance from the water table to the bottom of the enclosure structure after dewatering in the foundation pit, m; l_3 indicates the distance from the bottom of the enclosure structure to the impervious layer, m; and A, V, and L refers to the cross-sectional area of the seepage field, m^2, the total volume of seepage, m^3, and average seepage path, m, respectively.

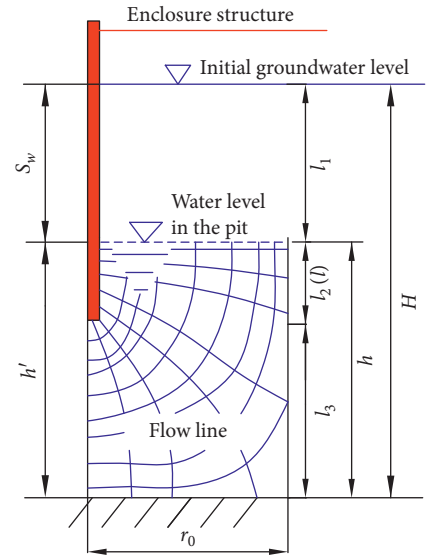

Figure 3: Seepage field distribution in the pit.

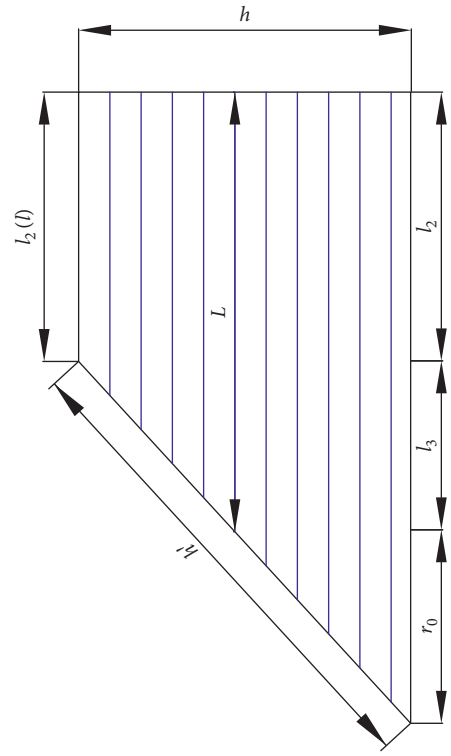

Figure 4: Simplification of the seepage path in the pit.

Simultaneous solution is obtained from equations (1) to (11), and then the following equation is obtained:

$$\frac{4\pi r_0^2\left(l_2 + l_3\right)\left(h' - h\right)}{\left(2l_2 + l_3 + r_0\right)^2} = \frac{0.3415\left[4H^2 - \left(H + h'\right)^2\right]}{\lg\left[1 + \left(\left(2\left(H - h'\right)\sqrt{Hk}\right)/r_0\right)\right] + \left(\left(H + h' - 2l\right)/2l\right)\lg\left(1 + \left(\left(H + h'\right)/10r_0\right)\right)}. \tag{12}$$

As for a real open cut foundation pit, it is seen from equation (12) that there is only one unknown variable in equation (12), that is, h', the water head at the bottom of the central axis of the enclosure structure inside the pit. This water head at the bottom of the central axis of the enclosure structure inside the pit can be iteratively obtained so that the radius of influence of dewatering in the foundation pit and the water inflow in the foundation pit can also be obtained.

2.2. Calculation of Dewatering in Foundation Pit in Multilayered Soil under Waterproofing Enclosure Structure. For the calculation of water inflow in the foundation pit considering the waterproofing effect of the enclosure structure under the geological conditions of the multilayered soil, the stratification calculation method is adopted to calculate the water inflow of each layer of soil separately, and algebraic calculation is performed to obtain the total water inflow in the pit. Generally speaking, there are many soil layers in actual foundation pits. It is very cumbersome and time-consuming to use this method. Therefore, the geological conditions of the multilayered soils are simplified to be a single formation, and the permeability coefficient is averaged for calculation. Three soil layers are used to illustrate this method as shown in Figure 5.

The permeability coefficient is calculated as follows:

$$k = \frac{k_1 h_1 + k_2 h_2 + k_3 h_3}{h_1 + h_2 + h_3}, \tag{13}$$

where h_1, h_2, and h_3 denote the thicknesses of the three soil layers, respectively, m, and k_1, k_2, and k_3 stand for the permeability coefficients, respectively, corresponding to the three soil layers, m/d.

2.3. Theoretical Design of Dewatering. In the actual project, the average permeability coefficient of the multilayered soils is firstly obtained according to equation (13), and then by using equation (12), engineering parameters are substituted and simplified to obtain the transcendental equation about h'. This equation can only be solved by means of a computer, so it is solved with Matlab using the dichotomy. By inputting the program in Matlab, the water head h' at the bottom of the central axis of the enclosure structure can be obtained, and then both the depth S_w of lowering water level in the well point and radius of influence R of the phreatic aquifer in foundation pit can then be obtained.

From equations (8) to (11), the equation for calculating the water inflow Q_1 in the pit is derived as follows:

$$Q_1 = \frac{kA(h' - h)}{L} = \frac{4k\pi r_0^2 (l_2 + l_3)(h' - h)}{(2l_2 + l_3 + r_0)^2}. \tag{14}$$

The water inflow of a single well is calculated as follows [18]:

$$q_0 = 120\pi r_s l \sqrt[3]{k}, \tag{15}$$

where q_0 represents the water inflow capacity of a single well, m^3/d; r_s denotes the filter radius, m; l stands for the length of the inlet part of the filter, m; and k denotes the permeability coefficient of the aquifer, m/d.

The number of dewatering wells is calculated as follows: according to the Chinese Technical Code for Groundwater Control in Building and Municipal Engineering (JGJ/T 111-2016) [19], if the safety level of the foundation pit is assessed to be in Grade I and the complexity of the foundation pit is evaluated to be complicated, and then the calculation coefficient ε in equation (16) gets the value of 1.2. The number of well points is obtained from the following equation:

$$n = \varepsilon \frac{Q_1}{q_0}, \tag{16}$$

$$D = \frac{L}{n}, \tag{17}$$

where D denotes the space between well points, m; L represents the circumference of the foundation pit, m; and n means the number of well points.

Therefore, the layout of the dewatering well points in the actual foundation pit can be obtained from the preceding equations.

3. Case Study of Dewatering in Foundation Pit

3.1. Engineering Background. This paper depends on a deep foundation pit of a subway station on Chengdu Metro Line 6. The station is an underground three-storied island platform station; its east side is closely adjacent to a street-facing commercial store that has 2-3 stories of brick-concrete structure. In addition, a 220 kV power cable tunnel constructed with conventional mining method is buried on its east side. The power cable tunnel is 1.4 m away from the sidewall of the station. The west side of the subway station closely approaches private houses and public shops on the ground surface, and the outer edge of a shop on the west side lies within a minimum distance of 1.7 m away from the foundation pit. The station is a 13.0 m wide island platform station with a standard cross-sectional width of 22.5 m, and its total length is 242.9 m long on the right side and 222.1 m long on the left side. The depth of the soil on its roof is about 3.98 m, and the depth of the bottom is about 26.64 m. The station and its surrounding environment are shown in Figure 6. According to the hydrogeological conditions for this project, there are two types of groundwater in the site: one is the perched water in the backfill layer above the clay layer, and the other is the pore water in the quaternary sand and pebble layer. The primary geotechnical investigation showed that stable water table measured in the site was 5.00~6.40 m in October 2015, and the detailed investigation showed that it was 5.40~6.70 m in October 2016. Obviously, there is minor difference in the two results of water tables, so the water level in the site is based on the results of the detailed geotechnical investigation. The site geotechnical properties and its distribution are also shown in Table 1.

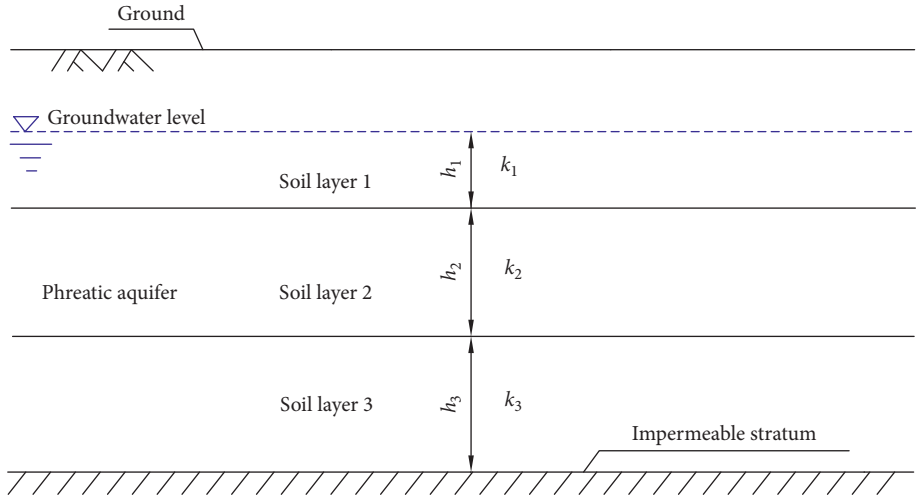

Figure 5: Geological conditions of multilayered soil.

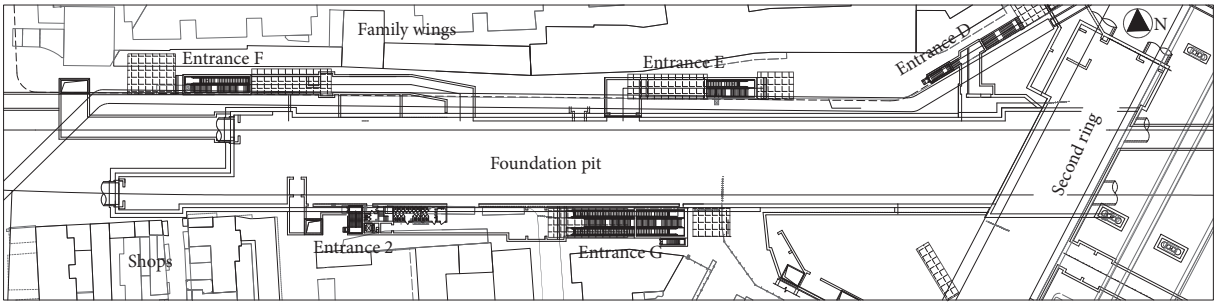

Figure 6: Station location and its surrounding environment.

Table 1: Soil properties and its distribution.

Sequence of strata	Name of stratum	Thickness of stratum (m)	Average thickness of stratum (m)	Soil permeability coefficient ($cm \cdot s^{-1}$)	Compression modulus ($\times 10^4$ kPa)
①	Miscellaneous fill	0.8~1.6	1.18	1.45×10^{-3}	2.8
②	Silty clay	0.5~2.3	1.17	5.79×10^{-5}	5.8
③	Clayey silt	0.5~1.2	0.73	1.74×10^{-4}	5.75
④	Fine sand	0.6~3.6	1.31	3.47×10^{-3}	5
⑤	Medium sand	0.3~1.5	0.69	1.16×10^{-2}	5.5
⑥	Loose pebble layer	1~1.6	1.3	2.55×10^{-2}	20
⑦	Slightly dense pebble layer	1~7.4	4.62	2.55×10^{-2}	23
⑧	Medium dense pebble layer	1~21.4	12.33	2.55×10^{-2}	32
⑨	Compacted pebble layer	Not drilled	Not drilled	2.55×10^{-2}	43

3.2. Design of Dewatering Well Points. Since the subway station is closely located to the shops and buildings on its two sides and the underground pipelines are densely packed in power cable tunnel and municipal sewages, there are no other spare places to install dewatering wells outside the foundation pit. Therefore, to avoid the impact of dewatering on the surrounding environment, well points are used to the lower groundwater level inside the foundation pit prior to its excavation.

The groundwater of the construction site belongs to the Quaternary existing in the sandy pebble pore phreatic aquifer. The thickness of the phreatic aquifer is less than 30 m, and the bottom floor of the station is located in the compacted pebble layer. The purpose of dewatering is to lower the water table in the foundation pit to 1 m below its bottom so that normal construction of the subway station can be fulfilled without groundwater. The open cut foundation pit of the station is 225 m long and 24 m wide with a

length-width ratio of 9.375 < 20. The depth of the foundation pit is about 26.64 m. For the convenience of calculation, it is set to 27 m. The diameter of the dewatering well is 600 mm, and the well bottom is 3.5 m lower than the one of the station. The length of the filter pipe is 2 m. The distance from the bottom of the filter pipe to the impervious layer is 2 m, and the stable water table is considered to be 6 m.

From the theoretical design and calculation of Section 2, it is known that 17 well points are to be laid around the foundation pit. Referring to the Chinese Technical Code for Groundwater Control in Building and Municipal Engineering (JGJ/T 111-2016) [19] and considering an idealized situation in which wells can be easily bored around the open cut foundation pit, the dewatering wells are arranged at the same distance along the foundation pit. After a well is installed at the center of the foundation pit, the remaining 16 well points are installed evenly at the inner edge of the pit. Since it is a long and narrow open cut foundation pit, the wells can be placed at the inner edge of the long side of the foundation pit, and the space between them is about 25 m. The specific layout of well points inside the open cut foundation pit is shown in Figure 7.

3.3. Comparison between Calculations with and without considering the Waterproof Effect of Enclosure Structure. According to the Chinese Technical Code for groundwater control in building and municipal engineering [18], if group well points are simplified to be large one, the total water inflow from the incomplete well points in the phreatic aquifer which is calculated by using equations (3) and (4) is replaced with the following equation:

$$h_m = \frac{H + h}{2}. \tag{18}$$

The parameters in equation (18) are the same as that in the formulae as stated above. If the waterproofing effect of the enclosure structure is not considered, then the depth of water level lowered by well points is expressed below:

$$S_w = H - h. \tag{19}$$

Substituting aforementioned engineering data into equations (3) and (16)–(18), respectively, it is seen that the water inflow from incomplete well point Q_3 in the foundation pit is

$$Q_3 = Q_2 = 12095.32\,\mathrm{m}^3, \tag{20}$$

the radius of influence of the foundation pit R' is

$$R' = 2S_w\sqrt{Hk} \approx 1052.33\,\mathrm{m}, \tag{21}$$

and the number of well points n' is certainly obtained according to

$$n' = 1.2\frac{Q_2}{q_0} \approx 23. \tag{22}$$

After a well point is installed at the center of the pit, the remaining 22 well points can then be set evenly at the edge of the foundation pit. Since it is a long and narrow foundation pit, the well points are evenly installed at the edge of the long side L of the foundation pit, and the space D' between them is

$$D' = \frac{L}{n} \approx 20.45\,\mathrm{m}. \tag{23}$$

Compared with the waterproofing effect of the enclosure structure, the water inflow in the foundation pit is 8936.5/12095.32 ≈ 0.74 times of the conventional algorithm proposed in the Chinese Specification, and the dewatering radius of influence is 540.99/1052.33 ≈ 0.51 times of the conventional algorithm in the Specification. The number of well points is 17/23 ≈ 0.74 times of the conventional algorithm in the Specification, and the space between them is 25/20.45 ≈ 1.22 times of the conventional algorithm in the Specification. Through comparison, if the enclosure structure of the foundation pit is used as a waterproof curtain, then the waterproofing effect of the enclosure structure should not be ignored when calculating water inflow inside the open cut foundation pit.

3.4. Arrangement of Points Monitoring Ground Subsidence. In order to make further analysis on the ground subsidence caused by dewatering in the foundation pit, the ground subsidence of the typical positions around the foundation pit is monitored. The ground subsidence monitoring points are set up according to the actual condition of the open cut foundation pit. In the actual project, the ground subsidence monitoring points are arranged around the foundation pit. For the consideration of symmetry and the convenience of measuring, six points at the midline of the long side of the foundation pit are selected, and they are 16-6, 16-5, 16-4, 16-3, 16-2, and 16-1, respectively; the distance between the well points and pit wall is set within 8 m, 12 m, 16 m, 20 m, 24 m, and 28 m, respectively. The monitoring points are shown in Figure 8, which are located at the center axis of the edge line of the pit. Step-by-step dewatering is carried out in the actual project, and the depth of dewatering for every step is set to 6 m, 5 m, 5 m, and 6 m respectively, and the total step amounts to 22 m.

4. Theoretical Calculation of Ground Subsidence Caused by Dewatering in Foundation Pit

4.1. Normative Calculation of Ground Subsidence Caused by Dewatering in Foundation Pit

4.1.1. Dupuit's Assumption and Derivation of Dewatering Funnel Curve. Dewatering in the foundation pit will definitely produce a falling funnel curve around the pit, and the groundwater may flow into the dewatering well inside the foundation pit. French scholar Dupuit first studied the steady well flow, put forward Dupuit's assumption, and derived the dewatering funnel curve. The hypothesis considers a cylindrical homogeneous phreatic aquifer with isotropic and horizontally waterproofing bottom floor, a fixed water head outside the aquifer, a complete pumping well in the center, no vertical infiltration recharge and

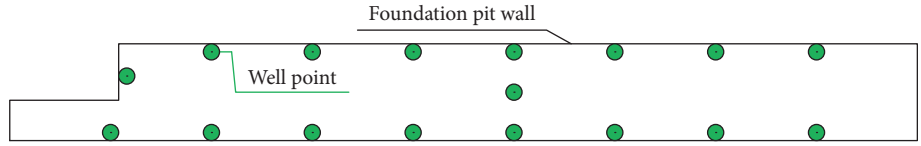

Figure 7: Schematic diagram of the layout of the dewatering well.

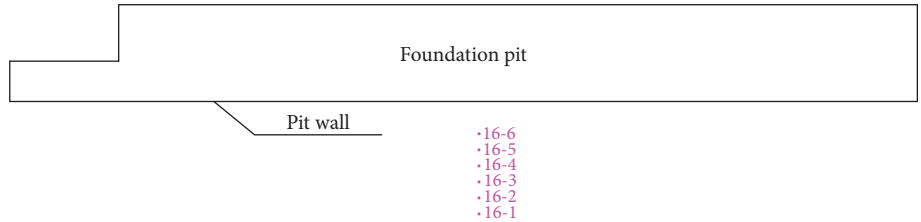

Figure 8: Schematic diagram of the ground subsidence monitoring points around the foundation pit.

evaporation, and a steady seepage subject to the linear law [20]. The dewatering well point can develop a dewatering funnel curve around it. Groundwater flows to the well after a certain time, and the dewatering curve can reach a steady state. Assuming that the well point dewatering is a stable phreatic well flow without the group well effect, the center of the well bottom is set to be the origin, and the abscissa is set to be the positive x-axis, as shown in Figure 9.

According to Dupuit's assumption, the water flow equation of the stable phreatic well is obtained below [20]:

$$Q = kIA = 2\pi rhk\frac{\mathrm{d}h}{\mathrm{d}r}. \tag{24}$$

If we separate the variable in equation (24) and take any one point on the dewatering funnel curve, then following equations are obtained by integrating the equation from the point to its boundary:

$$\left\{\begin{array}{l} r = x, h = z \\ r = R, h = H \end{array}\right\} \longrightarrow \int_x^R \frac{Q}{2\pi k}\frac{1}{r}\mathrm{d}r = \int_z^H h\,\mathrm{d}h, \tag{25}$$

and then,

$$\frac{Q}{2\pi k}\ln\frac{R}{x} = \frac{1}{2}\left(H^2 - z^2\right). \tag{26}$$

If the boundary condition meets

$$\begin{array}{l} x = r_0, \\ z = h_0 + l, \end{array} \tag{27}$$

and substituting equation (27) into equation (26), then the following equation is obtained:

$$\frac{Q}{2\pi k}\ln\frac{R}{r_0} = \frac{1}{2}\left[H^2 - \left(h_0 + l\right)^2\right]. \tag{28}$$

The solution of simultaneous equations (26) and (28) is used to obtain the following dewatering funnel curve equation of the well point:

$$z^2 = H^2 - \left[H^2 - \left(h_0 + l\right)^2\right]\frac{\ln\left(R/x\right)}{\ln\left(R/r_0\right)}, \tag{29}$$

where r_0 denotes the radius of wells, m; h_0 represents the length of the inlet part of the filter pipe, m; R denotes the radius of influence, m; H represents the height from the bottom of the well to the initial groundwater level, m; k is the permeability coefficient of the aquifer, m/d; A is the side area of the dewatering well, m^2; I denotes the groundwater seepage field hydraulic gradient; Q stands for the borehole water yield, m^3/d; and l means the distance between the bottom of well and the impermeable layer, m. The remaining symbols are shown in Figure 9.

4.1.2. Ground Subsidence at Any Point outside the Foundation Pit. At present, the calculation of ground subsidence around the foundation pit after dewatering is generally carried out using the stratification summation method given in the Technical Specification for Retaining and Protection of Building Foundation Excavations (JGJ 120-2012) [18]. The ground subsidence can be calculated by summarizing the compression of each layer of soil. Firstly, we can calculate the additional effective stress caused by dewatering and then calculate the ground subsidence using stress calculation:

(1) When the soil layer numbered as i is above the initial groundwater level, the effective stress is

$$\Delta\sigma'_{z_i} = 0. \tag{30}$$

(2) If the soil layer numbered as i is located between the postdewatering groundwater level and the initial groundwater level, then the effective stress is

$$\Delta\sigma'_{z_i} = \gamma_w z, \tag{31}$$

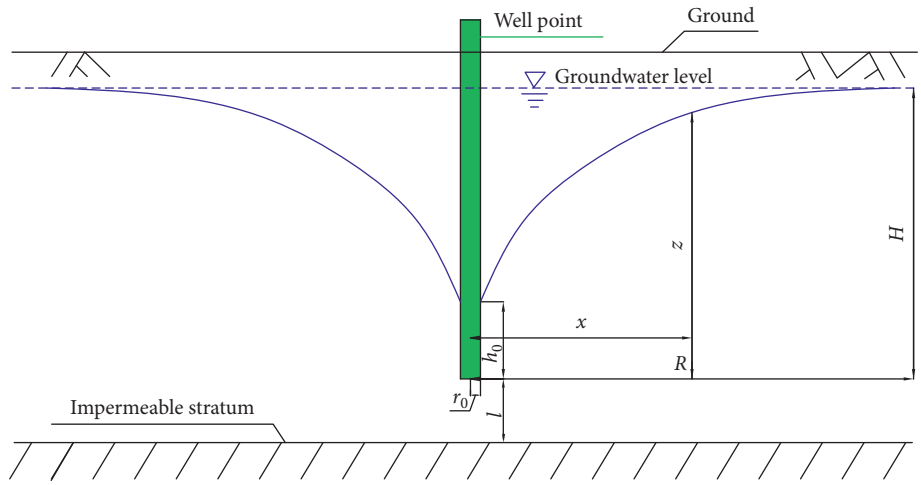

Figure 9: Dewatering funnel curve for the phreatic incomplete well point.

(3) When the soil layer numbered as i is below the groundwater level after dewatering, then the effective stress is

$$\Delta\sigma'_{z_i} = \lambda_i \gamma_w s_i. \tag{32}$$

The soil compression caused by dewatering is as follows:

$$s = \psi_w \sum \frac{\Delta\sigma'_{z_i} \Delta h_i}{E_{s_i}}, \tag{33}$$

where γ_w means the bulk density of water, kN/m^3; z denotes the vertical distance from the midpoint of the soil layer i to the initial groundwater level, m; and λ_i represents the calculation coefficient, it should be based on the analysis of groundwater seepage. If the analysis data are not available, then its value should be based on local engineering experience; s_i refers to the depth of lowering groundwater level corresponding to the calculation profile, m; s denotes the ground compression in the calculation profile, m; and ψ_w means the empirical coefficient of subsidence calculation based on local engineering experience. If no experience is available, then the value is set to be 1; $\Delta\sigma'_{z_i}$ denotes the mean additional stress of the soil layer i under the ground surface caused by dewatering, kPa; Δh_i means the thickness of the soil layer i, m; and E_{s_i} denotes the compressive modulus of the soil layer i, kPa.

4.2. Calculation of Ground Subsidence Caused by Dewatering in Foundation Pit under Seepage Force. The pumping and drainage of the dewatering well will cause the change of the underground seepage field, which will generate a new seepage field and lead to the variation of the stress field around the well. Therefore, the seepage force is the main cause of soil consolidation and settlement. The seepage of groundwater causes the dissipation of pore water pressure, resulting in an increase in effective stress. That is, additional stress is generated in the soil, the direction of which is vertically downward; in addition, it produces a horizontal component. Deformation can be caused by the impact of seepage force. The additional stress, namely, the vertical component of the seepage force, will cause the ground subsidence [21]. The horizontal component of the seepage force will cause the lateral deformation of the soil. According to reference [22], the seepage direction of any water head at any point is tangent to the phreatic surface at that point, pointing to the well axis, as shown in Figure 10.

Wu and Zhu [22] performed related research and proposed a new algorithm of ground subsidence caused by seepage force. Yang and Zhao [23] also used this method to calculate ground subsidence. This section draws lessons from their research to discuss the dewatering in open cut foundation pit of a subway station on Chengdu Metro Line 6.

The stratum is divided into three parts: dry soil zone, dewatered zone, and saturated zone. The dry soil zone is always above the groundwater level before and after dewatering, which does not contain groundwater and seepage force during dewatering. Thus, additional stress does not appear in this zone, and the subsidence value caused by dewatering is 0. The other two layers are S_1 and S_2, respectively, as shown in Figure 10. The soil layer S_1 in the dewatering process is drained. The zone S_2 is always below the groundwater level and is saturated. In this section, the soil subsidence in the dewatered and saturated zones is calculated separately. The seepage forces in these two areas possess horizontal components, as shown in Figure 10.

Assuming that the water head that keeps a distance of x_0 from itself to the well axis is z_0 as shown in Figure 10, according to the dewatering funnel curve equation (29) in Section 4.1, the height of the falling funnel curve is obtained. The direction of the seepage force is actually in the straight line vector on the curve which goes through the point (x_0, z_0) and is tangent to the falling funnel curve and points to the well. In order to find out the slope of the straight line, the following equation is obtained by performing the derivative of equation (29) at point $x = x_0$.

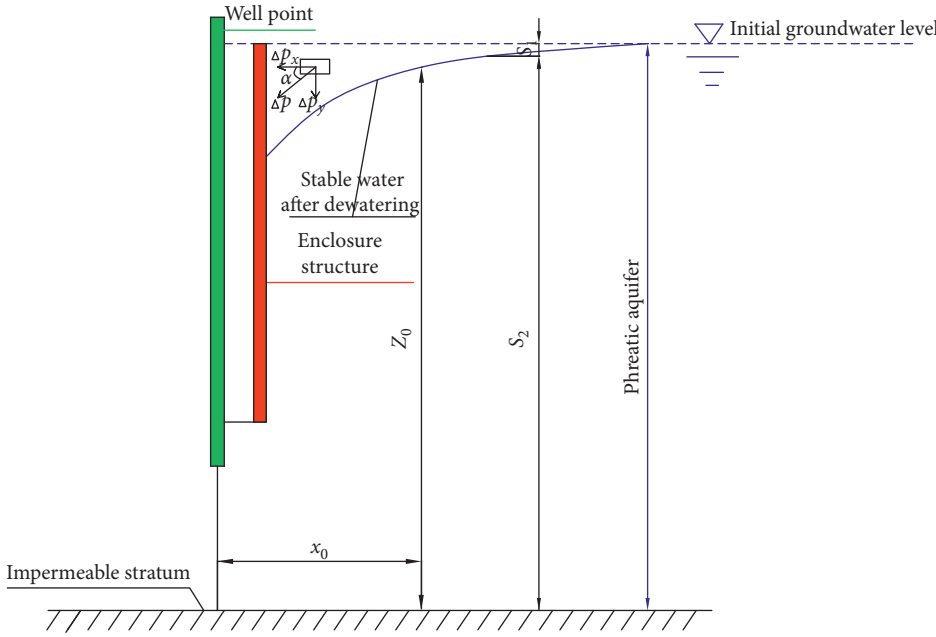

FIGURE 10: Simplified calculation model considering seepage force.

$$z'(x_0) = \frac{1}{2\sqrt{H^2 - \left[H^2 - (l+h_0)^2\right]\left(\ln(R/x_0)/\ln(R/r_0)\right)}} \cdot \frac{H^2 - (l+h_0)^2}{x_0 \ln(R/r_0)}. \tag{34}$$

The equation of the line that passes through the point (x_0, z_0) and is tangential to the curve after the dewatering becomes stable is assumed to be

$$y = x\tan\alpha + b. \tag{35}$$

The slope of the equation is

$$\tan\alpha = z'(x_0). \tag{36}$$

According to the trigonometric function conversion,

$$\sin\alpha = \frac{\tan\alpha}{\sqrt{1+\tan^2\alpha}}. \tag{37}$$

Then, the following equation is obtained:

$$\sin\alpha = \frac{z'(x_0)}{\sqrt{1+\left[z'(x_0)\right]^2}}. \tag{38}$$

Therefore, the vertical component of additional pressure of the surrounding stratum caused by dewatering in the foundation pit is expressed as

$$\Delta P_y = \Delta P \sin\alpha = \Delta P \frac{z'(x_0)}{\sqrt{1+\left[z'(x_0)\right]^2}}, \tag{39}$$

where ΔP_x denotes the horizontal component of the seepage force, ΔP_y denotes the vertical component of the seepage force, and ΔP is the seepage force.

The angle α in equation (39) denotes the one exists between the horizontal component of the additional pressure and the additional pressure caused by dewatering in the foundation pit.

Based on equations (30) to (33), the additional stresses in the dewatering zone and the saturation zone are calculated separately. The rewriting is carried out on the basis of equation (34), which derives the ground subsidence caused by dewatering in the foundation pit considering the action of seepage force. The formula after rewriting is as follows:

$$s = \psi_w \sum \frac{\Delta\sigma'_{z_i}\Delta h_i}{E_{s_i}} \frac{z'(x_0)}{\sqrt{1+\left[z'(x_0)\right]^2}}. \tag{40}$$

Substituting equation (34) into equation (40) yields the following equation:

$$s = \psi_w \sum \frac{\Delta\sigma'_{z_i}\Delta h_i}{E_{s_i}} \frac{H^2 - (l+h_0)^2}{\sqrt{\left[H^2 - (l+h_0)^2\right] + 4x_0^2\left(\ln(R/r_0)\right)^2\left\{H^2 - \left[H^2 - (l+h_0)^2\right]\left(\ln(R/x_0)/\ln(R/r_0)\right)\right\}}}. \tag{41}$$

If the ground subsidence S_1 and S_2 corresponding to the dewatered and saturated zones are separately figured out, then the total ground subsidence is obtained and illustrated in the following equation:

$$S = S_1 + S_2, \tag{42}$$

where the symbols are illustrated in Section 4.1.

5. Numerical Simulation

With fast development of urban construction, various infrastructures such as subway station, high-speed railway tunnel, underground parking lot, and basement are being built, especially the construction of deep foundation pits. The geological condition varies in the foundation pit, and the surrounding environment is becoming more and more complex after construction. Theoretical analysis and empirical calculation methods are no longer suitable for practical projects. Nowadays, actual projects are generally built ahead of theoretical research, and calculation methods of numerical simulation provide an effective approach for the design and construction of practical foundation pit. Although numerical simulation method has not been proposed for very long time, it has become the most common method used in structural analysis and calculation so far. Many scholars [24–31] have also used FLAC^{3D} to conduct fluid-solid coupling analysis of dewatering in the foundation pit. Finite difference software FLAC^{3D} is also employed in this paper to carry out three-dimensional numerical simulation of the whole process of the environment change caused by dewatering in the open cut foundation pit of a metro station on Chengdu Metro Line 6. The calculation results are compared with the one obtained from theoretical calculation and on-site monitoring, which are used to make further study on the surrounding ground subsidence due to dewatering in the open cut foundation pit.

5.1. Physical and Mechanical Parameters. According to the geological properties of the actual project, the calculation parameters are obtained and shown in Table 2.

5.2. Establishment of 3D Model and Initial Stress Balance. Based on the engineering geological and hydrological conditions, a three-dimensional stratigraphic model is established. From the geological section of the site (Figures 11 and 12), it can be seen that each of soil layers is nearly horizontal and almost parallel to each other. So, in order to establish the model and conduct the calculation conveniently [26], the geological layers in the model are simplified. The foundation pit and wells are set up in the stratigraphic model according to dewatering scheme. According to the principle of Saint Venant in elastic mechanics, in order to eliminate the boundary influence of the foundation pit on calculation results, the calculation model is extended to 3~5 times of the depth of the pit from the periphery of the foundation pit on the plane. The depth is set to the impervious interface, and the entire calculation domain is in the volume of $420\,\text{m} \times 198\,\text{m} \times 72\,\text{m}$. Referring to geotechnical mapping and geological properties, the model is divided into 9 strata, and the generalized permeability coefficient and stratum thickness are shown in Table 1.

According to stratum distribution and initial conditions, the calculation domain is divided into grids by considering the monitoring points, the dewatering wells, and the diaphragm wall considering the geological survey. In the meshing, the grid of the calculation domain is locally refined; in addition, the grids around the foundation pit are also refined, but grids far away from the pit are sparsely meshed considering Saint Venant's principle [26]. So the entire model is then divided into 42 layers, 78 rows, 300 columns, and a total of 982,800 elements, and the established three-dimensional model is shown in Figure 13.

After the 3D model is set up, the initial stress balance is needed to be applied firstly and the corresponding seepage and displacement boundary conditions are also applied. The normal displacement and the bottom displacement of the four sidewalls and bottom of the model are restricted, and the horizontal displacement of the wall of the dewatering well is also constrained. The bottom filter pipe of the dewatering well belongs to the seepage boundary, which is achieved by applying the pore water pressure. After numerical simulation, the pore water pressure of initial equilibrium is shown in Figure 14. The pore water pressure in the initial state is evenly applied on the strata.

5.3. Numerical Simulation of Fluid-Solid Coupling of Ground Subsidence Caused by Dewatering in Foundation Pit. After the initial equilibrium of the numerical model, the effect of single well and group wells were firstly carried out separately. The stepwise dewatering was conducted under the conditions of single well and group wells separately without considering excavation. The calculated isograms of the dewatering at all levels and the subsidence of the monitoring points are analyzed.

5.3.1. Numerical Simulation Analysis of Single Well Dewatering. Considering the symmetry of the well point, the well point at the center of the calculation domain is selected when carrying out single well simulation. The position of the single well on the model is shown in Figure 15. The isograms showing subsidence and pore water pressure at various drawdowns are also shown in Figures 16–23.

It is seen from Figures 16–23 that the influence range of dewatering well increases with the increase of drawdown. After the well is dewatered, the pore water pressure forms the dewatering funnel surface. The bigger the drawdown is, the deeper the surface becomes. Moreover, due to the waterproofing effect of the diaphragm wall, the stratum inside the pit bulges, but the stratum outside the pit subsides. This is because the groundwater flows through the bottom of the diaphragm wall into the pit. The increase of the pore water pressure in the pit causes the additional stress to increase, which leads to the upheaval of the soil layer in the pit. The decrease of the pore water pressure outside the pit causes the effective stress of the outer stratum to decrease, resulting in the formation of downward additional stress in the outer

Table 2: Physical and mechanical parameters of strata.

Name of stratum	Modulus of deformation E (MPa)	Poisson's ratio	Density (g/cm^3)	Permeability coefficient (m/d)
Miscellaneous fill	2	0.35	1.8	1.25
Silty clay	4	0.29	1.96	0.05
Clayey silt	4	0.30	1.94	0.15
Fine sand	4	0.28	1.85	3
Medium sand	4.0	0.26	1.9	10
Loose pebble layer	18	0.25	2	22
Slightly condensed pebble layer	20	0.23	2.1	22
Medium condensed pebble layer	28	0.20	2.2	22
Compacted pebble layer	38	0.17	2.3	22

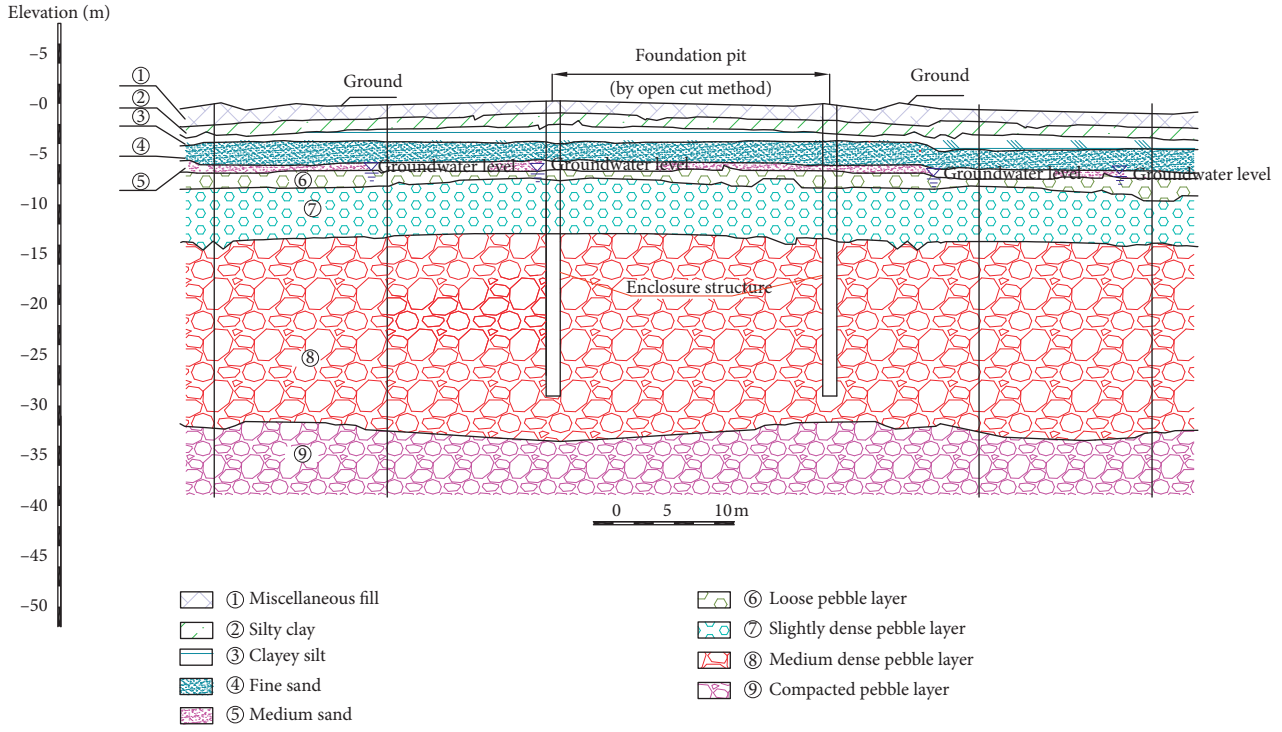

Figure 11: Geological section of the territory.

stratum of the pit, which eventually leads to the consolidation and settlement of the outer stratum.

5.3.2. Numerical Simulation Analysis of Group Wells Dewatering. When conducting the effect of group wells on ground subsidence, the calculation is based on the well point layout diagram designed in Section 3. The layout of the group wells in the model is shown in Figure 24. The isograms showing ground subsidence and pore water pressure calculated using FLAC^{3D} are shown in Figures 25–32.

It is seen from the isograms shown in Figures 25–32 that the deeper the groundwater drawdown, the greater the impact on the surrounding ground is, and the lower the funnel surface formed by the pore water pressure. Compared with the isogram under the effect of single well in Section 5.2, the influence of dewatering by group wells is much larger. Group wells dewatering has a great impact on the pore water pressure and strata deformation inside the foundation pit; that is, the influence of group wells on ground subsidence inside the pit is obvious and should not be ignored. The subsidence and pore water pressure isogram under different drawdowns are symmetrically distributed. As shown in the single well effect, the strata inside the foundation pit bulge during the dewatering of group wells, but the strata outside the foundation pit subside. This is mainly due to the result of the movement of groundwater outside the pit to the dewatering well inside the pit.

5.3.3. Effect of Group Wells. According to the results obtained from 3D simulation, the subsidence of the six monitoring points on the sides of the foundation pit due to different drawdowns caused by the single well and the group wells are shown in Figure 33.

Grade I drawdown, including Grade II, Grade III, and Grade IV drawdown, means that the dewatering depth of groundwater level is in 6 m, 11 m, 16 m, and 22 m, respectively.

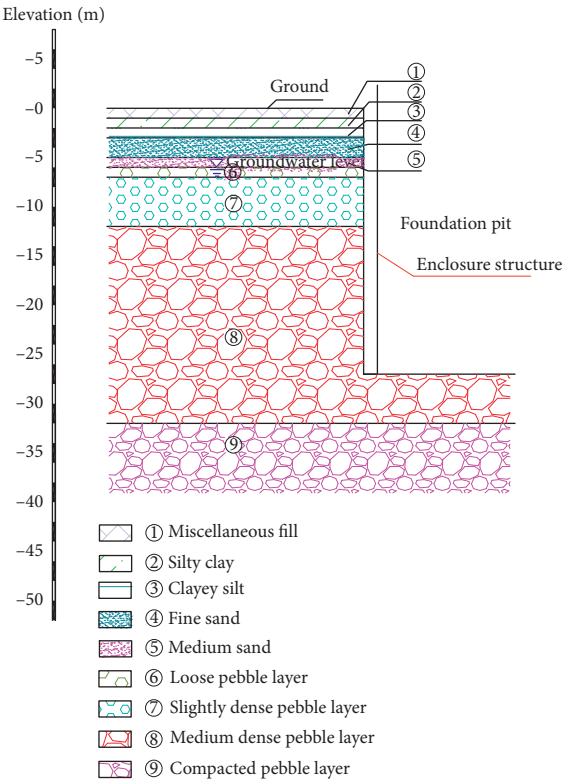

Figure 12: Geological profile of the strata and foundation pit.

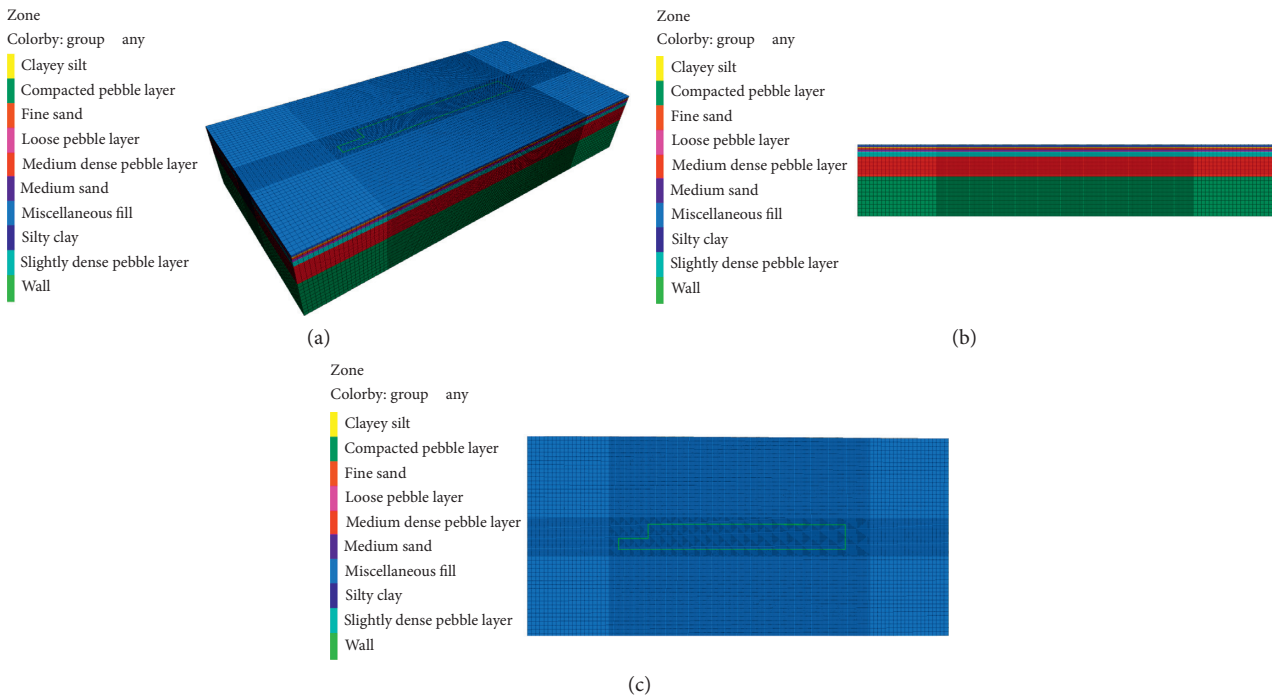

Figure 13: 3D model of the foundation pit and soil strata. (a) Model mesh diagram. (b) Model cross section. (c) Model top view.

The curves of both single well and group wells under different drawdowns are similar, and the farther the monitoring point is away from the well axis in foundation pit, the smaller the ground subsidence becomes. The greater the depth of groundwater is lowered at the same monitoring point, the greater the ground subsides. The maximum settlement after

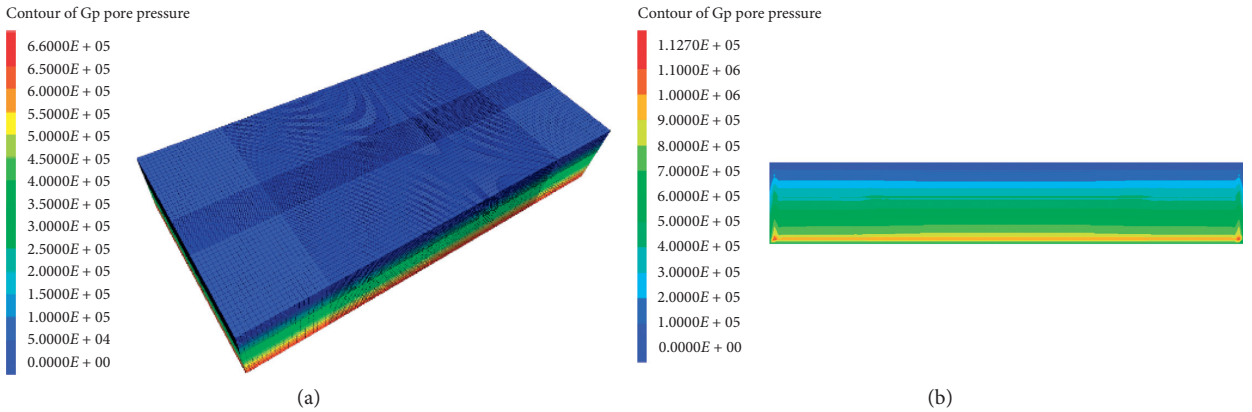

Figure 14: Initial pore water pressure nephogram (unit: Pa). (a) Three-dimensional diagram. (b) Model cross section.

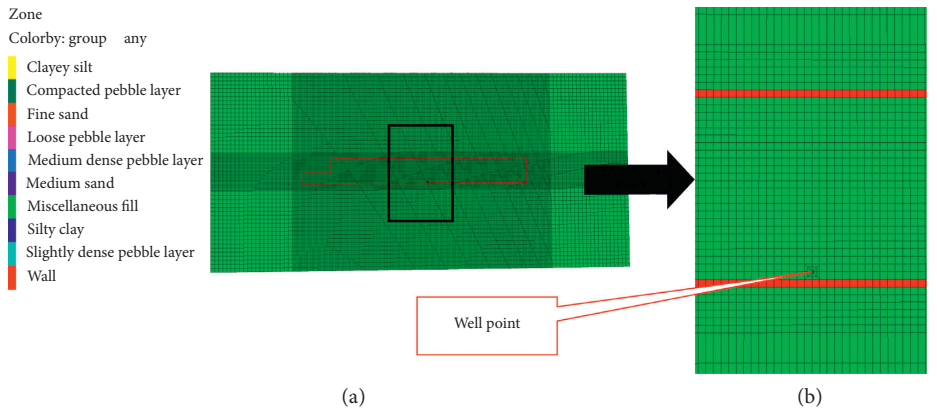

Figure 15: Layout of the single well model.

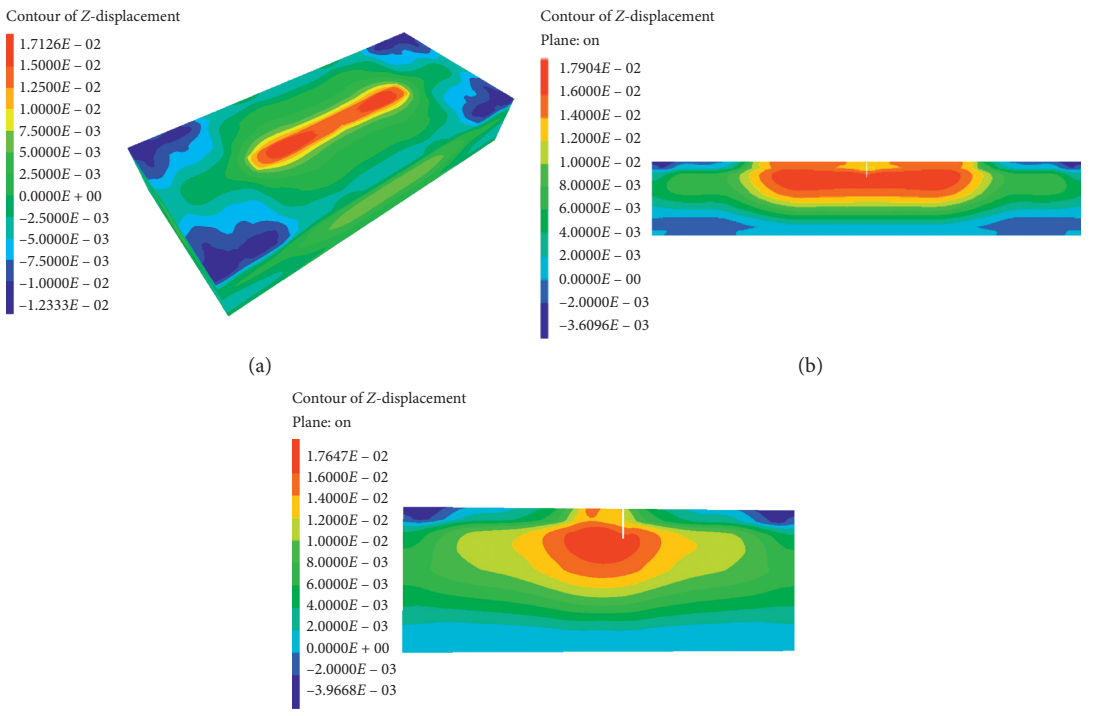

Figure 16: Single well subsidence nephogram after the first drawdown (unit: m). (a) Three-dimensional diagram. (b) Cross section of the well midpoint. (c) Longitudinal section of the well midpoint.

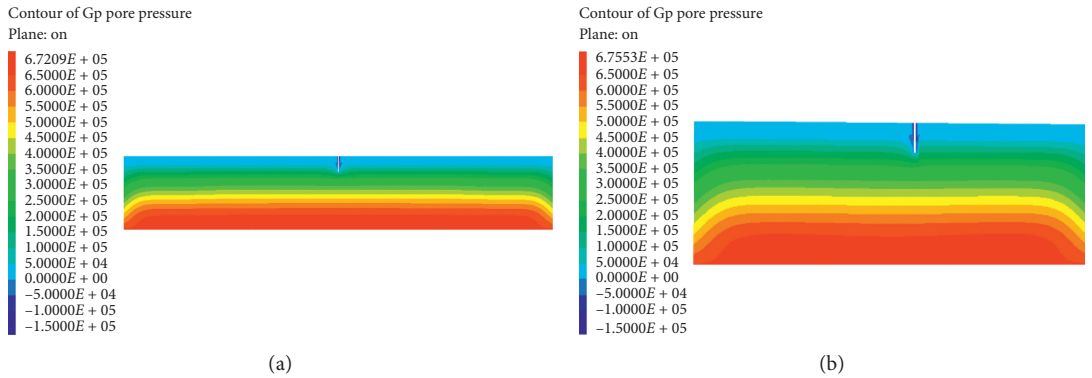

Figure 17: Single well pore water pressure nephogram after the first drawdown (unit: Pa). (a) Cross section of the well midpoint. (b) Longitudinal section of the well midpoint.

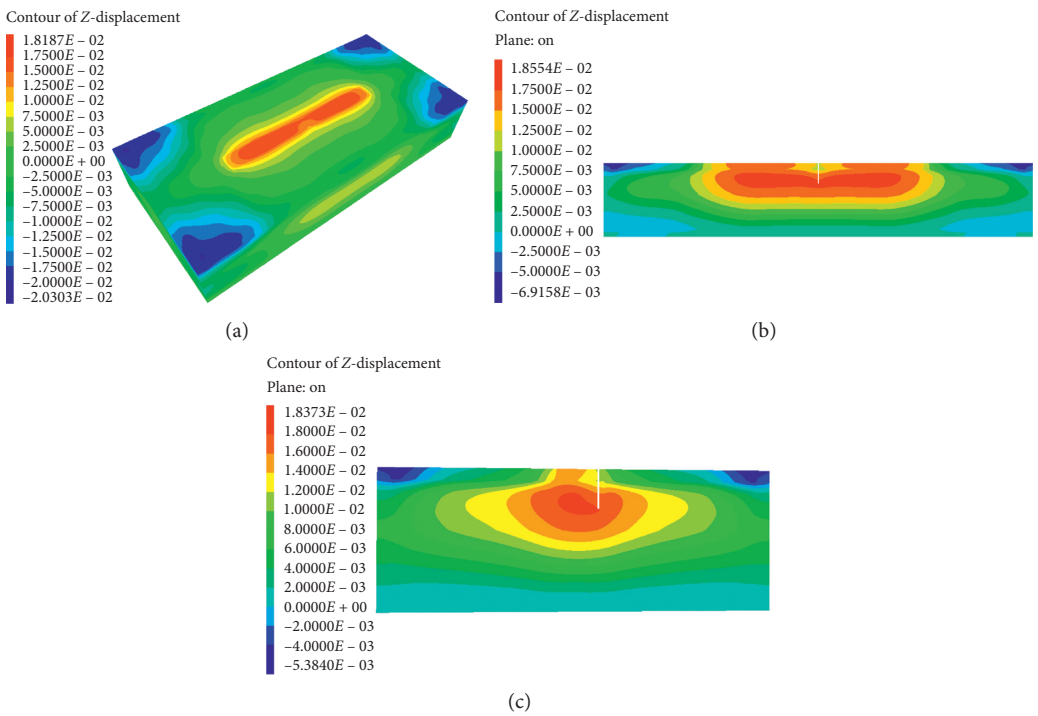

Figure 18: Single well subsidence nephogram after the second drawdown (unit: m). (a) Three-dimensional diagram. (b) Cross section of the well midpoint. (c) Longitudinal section of the well midpoint.

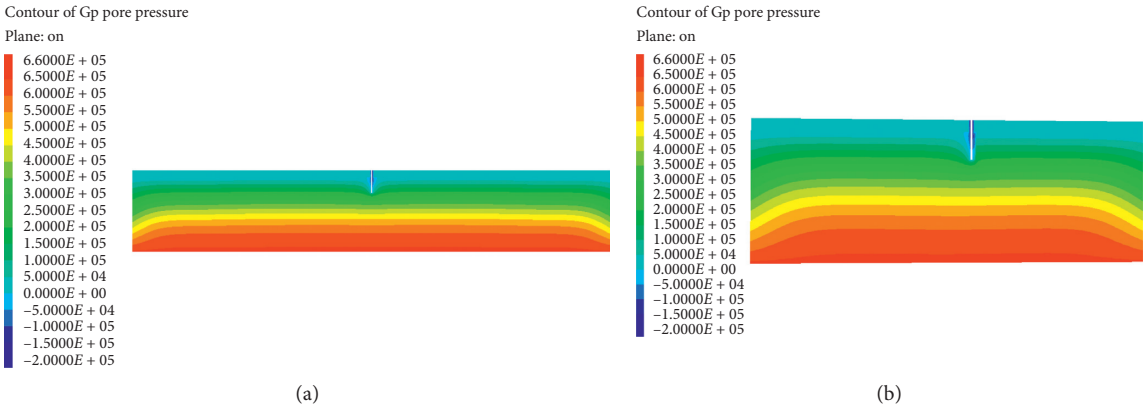

Figure 19: Single well pore water pressure nephogram after the second drawdown (unit: Pa). (a) Cross section of the well midpoint. (b) Longitudinal section of the well midpoint.

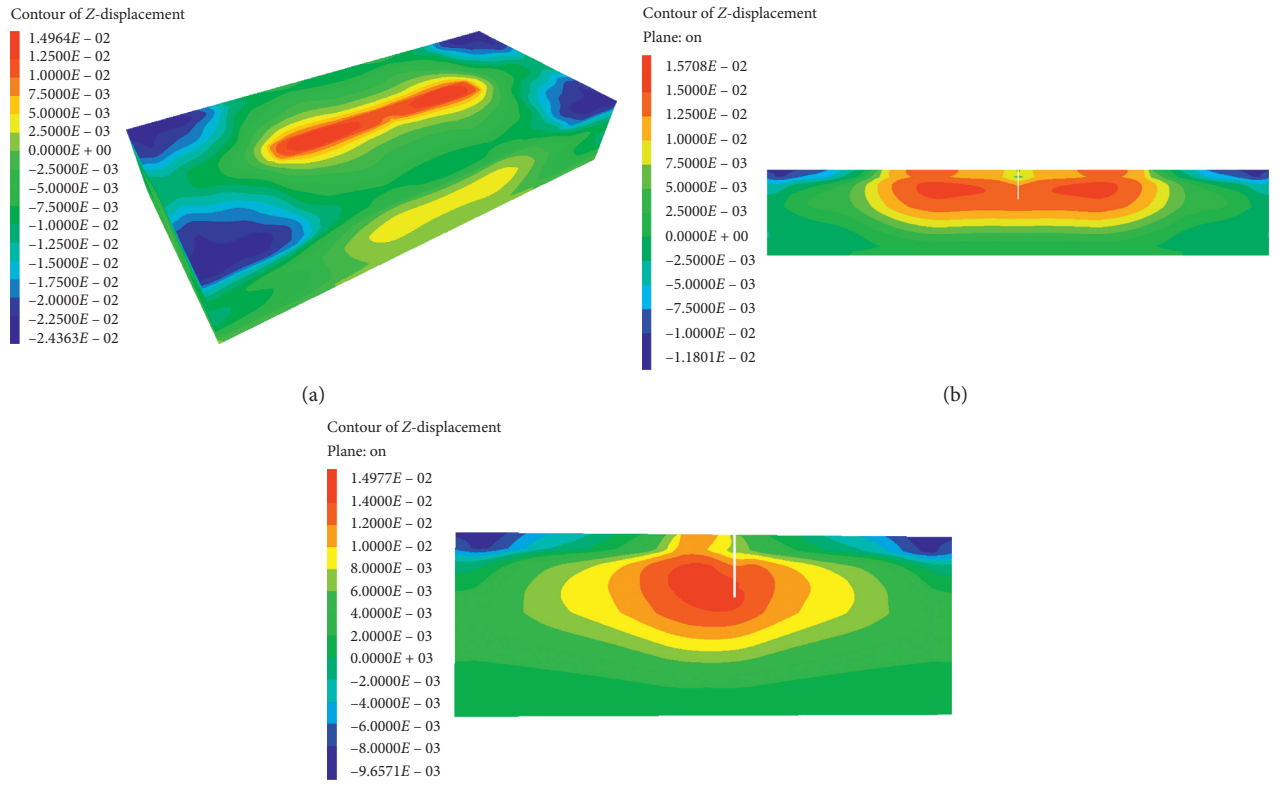

Figure 20: Single well subsidence nephogram after the third drawdown (unit: m). (a) Three-dimensional diagram. (b) Cross section of the well midpoint. (c) Longitudinal section of the well midpoint.

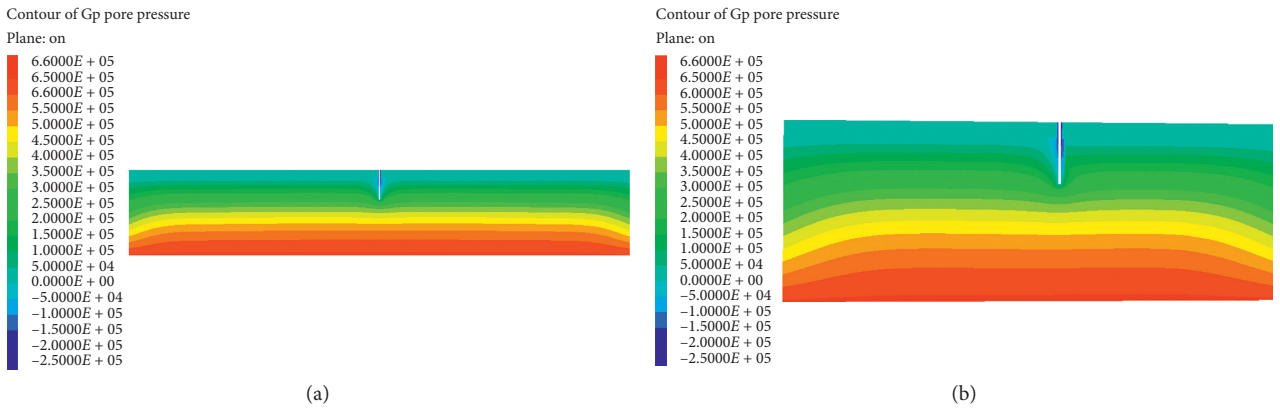

Figure 21: Single well pore water pressure nephogram after the third drawdown (unit: Pa). (a) Cross section of the well midpoint. (b) Longitudinal section of the well midpoint.

single well dewatering is about 4.46 mm, and the maximum settlement after group wells dewatering reaches 4.8 mm. The subsidence of the monitoring points that are far away from the well axis are basically the same, this occurs under single well and group wells. Generally, ground subsidence around the well after group wells dewatering is slightly larger than that after single well dewatering, but the increment is very small. Moreover, as the distance from the well axis is farther, the increase effect is less obvious. It is also seen that the ground subsidence caused by group wells dewatering inside the foundation pit is not obvious, especially when the distance from the foundation pit is faraway or the drawdown is not large. Therefore, in order to facilitate research, the group wells effect can sometimes be simplified into single well effect in geotechnical engineering. Therefore, through FLAC^{3D} numerical simulation, it is found that the group well effect on

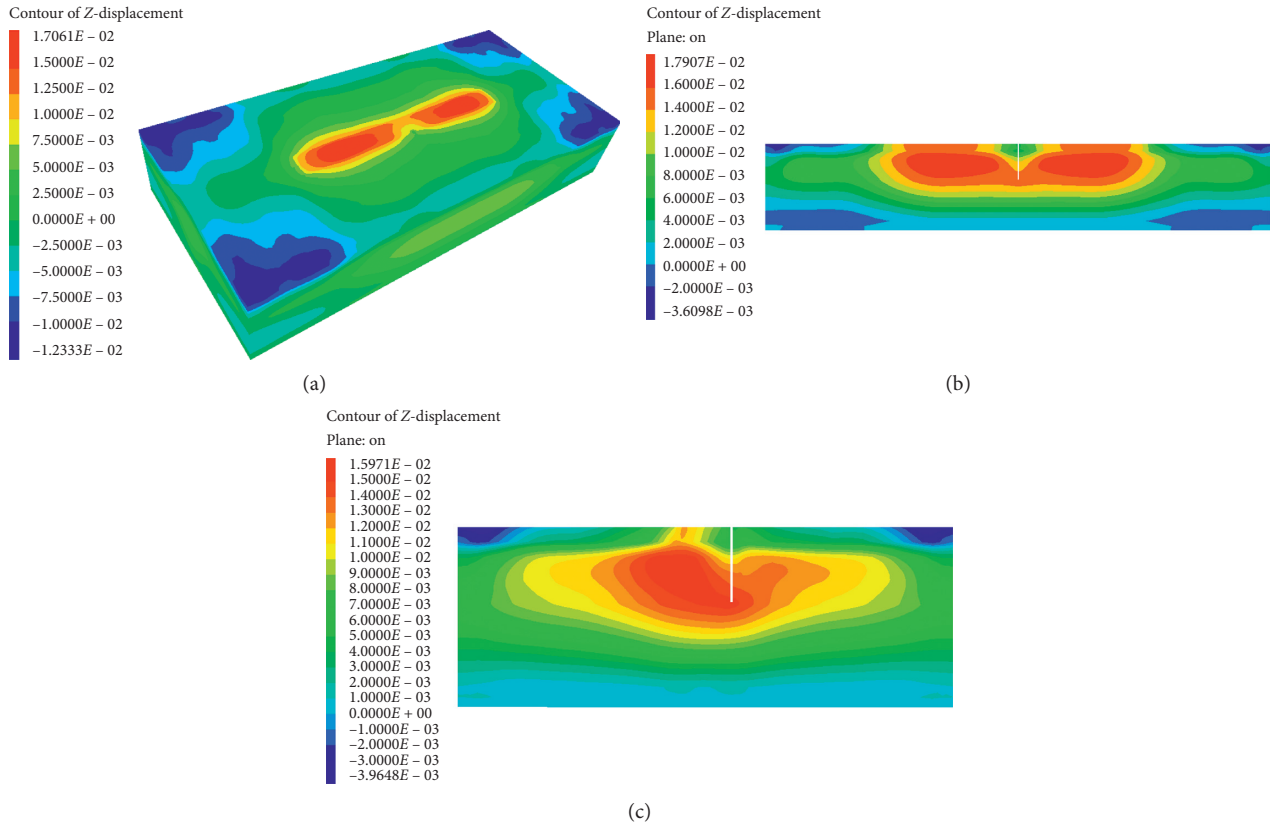

Figure 22: Single well subsidence nephogram when the drawdown is stable (unit: m). (a) Three-dimensional diagram. (b) Cross section of the well midpoint. (c) Longitudinal section of the well midpoint.

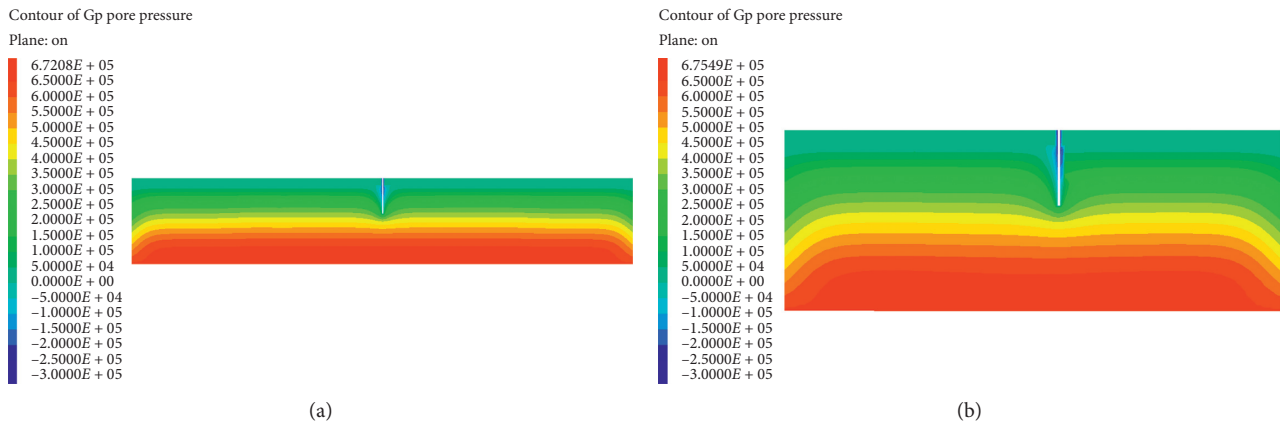

Figure 23: Single well pore water pressure nephogram when the drawdown is stable (unit: Pa). (a) Cross section of the well midpoint. (b) Longitudinal section of the well midpoint.

ground subsidence is not obvious, so for the convenience of calculation, the group well effect can be ignored while designing dewatering wells for open cut foundation pit.

5.4. Comparative Analysis of Subsidence due to Dewatering. Based on the improved settlement calculations under the action of seepage force, three calculation methods including the conventional algorithm proposed in the Chinese Specification, the on-site monitoring, and the numerical simulation are used in the paper, and the ground subsidence around the foundation pit under different drawdowns in the context of the project is obtained. The comparison of ground subsidence due to different drawdowns is illustrated in Figure 34.

It is seen from Figure 34 that the overall trend under different conditions fits the on-site monitoring results. The results obtained from theoretical analysis considering the effect of seepage force and numerical simulation are much

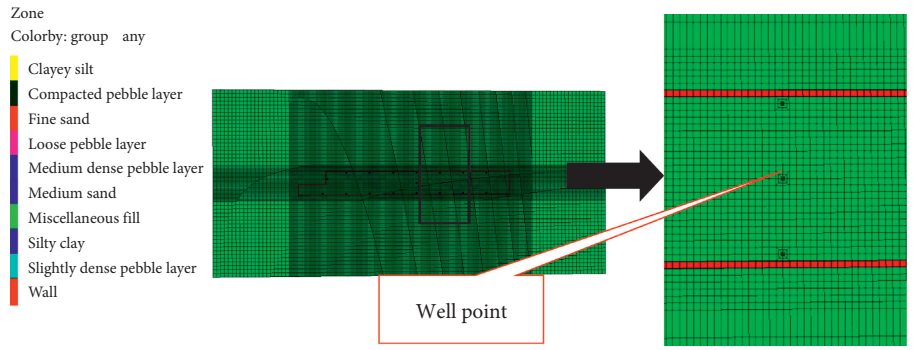

Figure 24: Layout of group wells in the model.

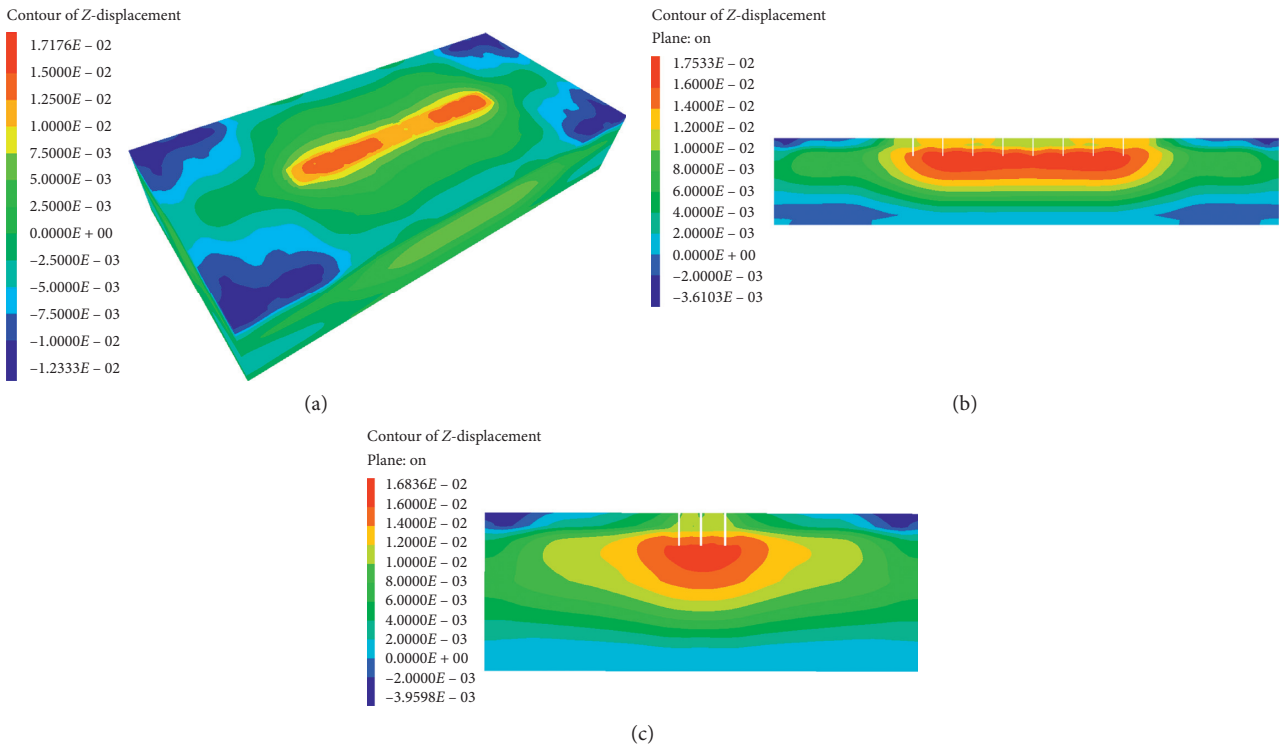

Figure 25: Group wells subsidence nephogram after the first drawdown (unit: m). (a) Three-dimensional diagram. (b) Cross section of the well midpoint. (c) Longitudinal section of the well midpoint.

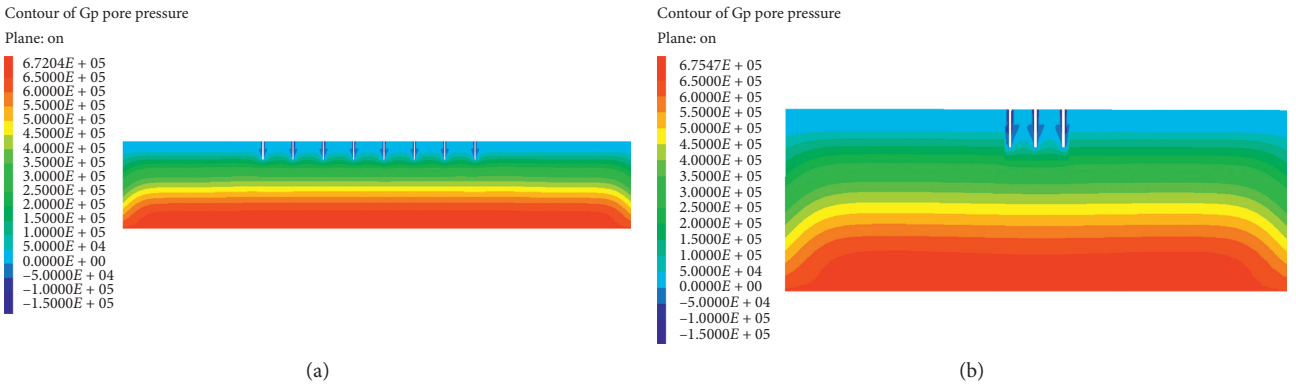

Figure 26: Group wells pore water pressure nephogram after the first drawdown (unit: Pa). (a) Cross section of the well midpoint. (b) Longitudinal section of the well midpoint.

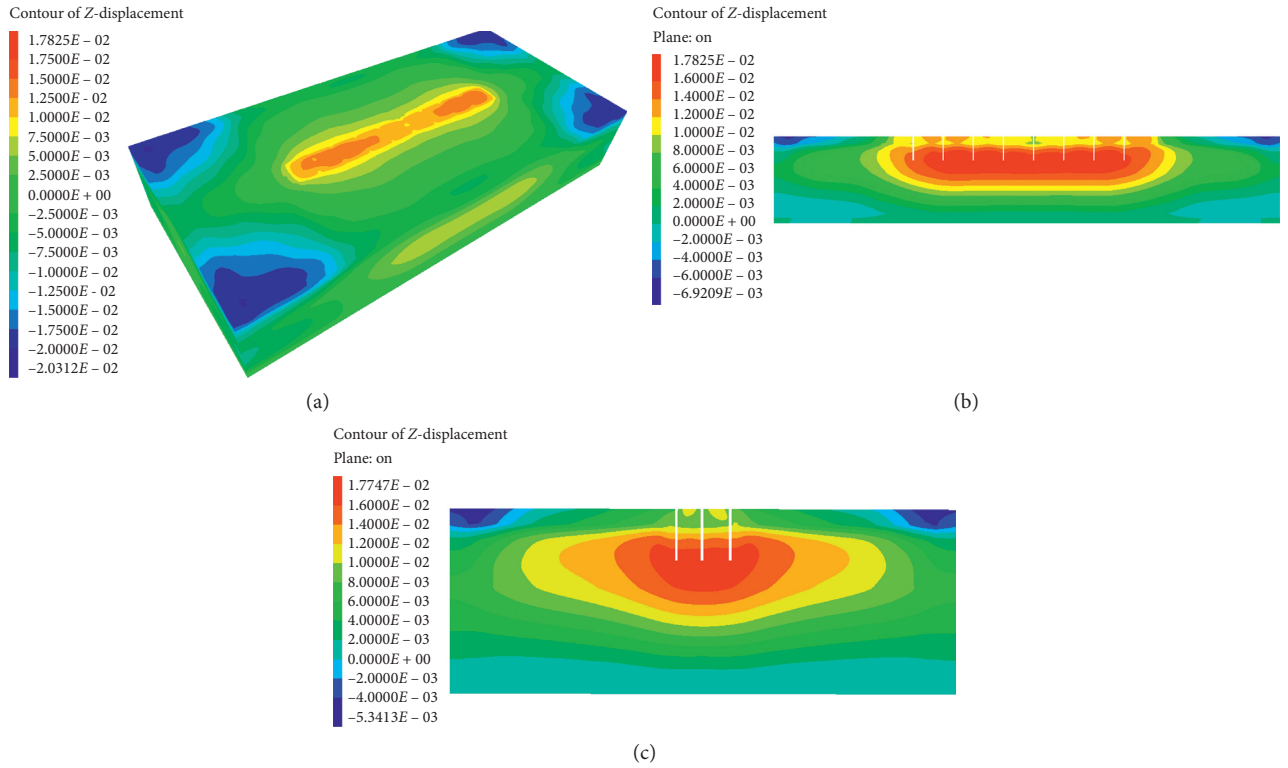

Figure 27: Group wells subsidence nephogram after the second drawdown (unit: m). (a) Three-dimensional diagram. (b) Cross section of the well midpoint. (c) Longitudinal section of the well midpoint.

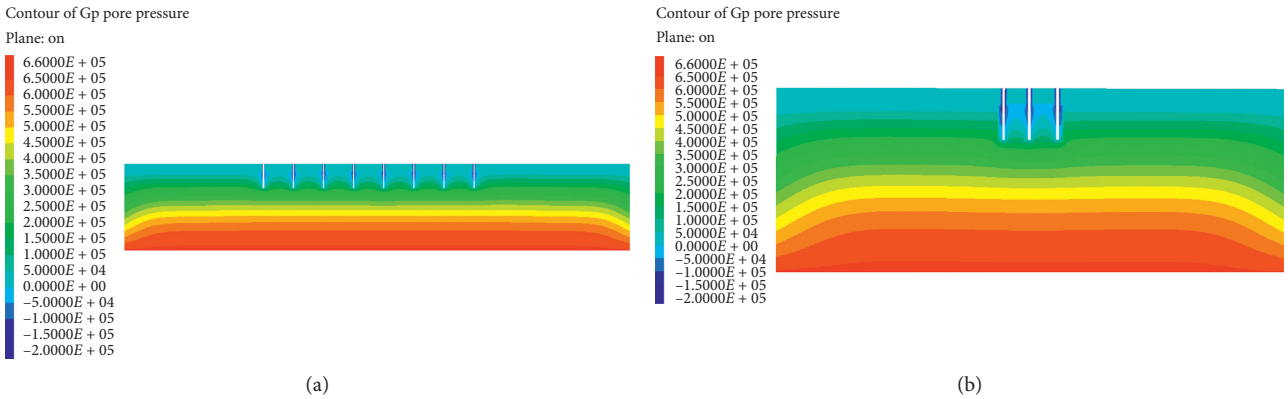

Figure 28: Group wells pore water pressure nephogram after the second drawdown (unit: Pa). (a) Cross section of the well midpoint. (b) Longitudinal section of the well midpoint.

closer to the ones of the field monitoring. Moreover, the theoretical calculation and numerical simulation values are much closer to the on-site monitoring values, but there is a large gap between the normative calculation and the on-site monitoring values. The greater the depth of groundwater dewatering is, the larger the groundwater jumps, and the actual stable dewatering curve is higher than Dupuit's falling funnel curve. However, the group wells effect of ground subsidence around the foundation pit is obvious at high drawdown. Therefore, as the depth of groundwater extraction is larger, the effect of group wells and the depth of dewatering should be considered in the calculation of ground subsidence. The farther the point is away from the foundation pit, the smaller the difference is in settlement values calculated by each calculation method. Considering the deformation of the soil layer caused by dewatering is not only the vertical deformation, but also the lateral deformation, when the vertical deformation is only considered, the calculation results may reach the on-site monitoring values. By considering the calculation under the action of seepage force, the settlements of the ground around the foundation pit caused by dewatering at different drawdowns

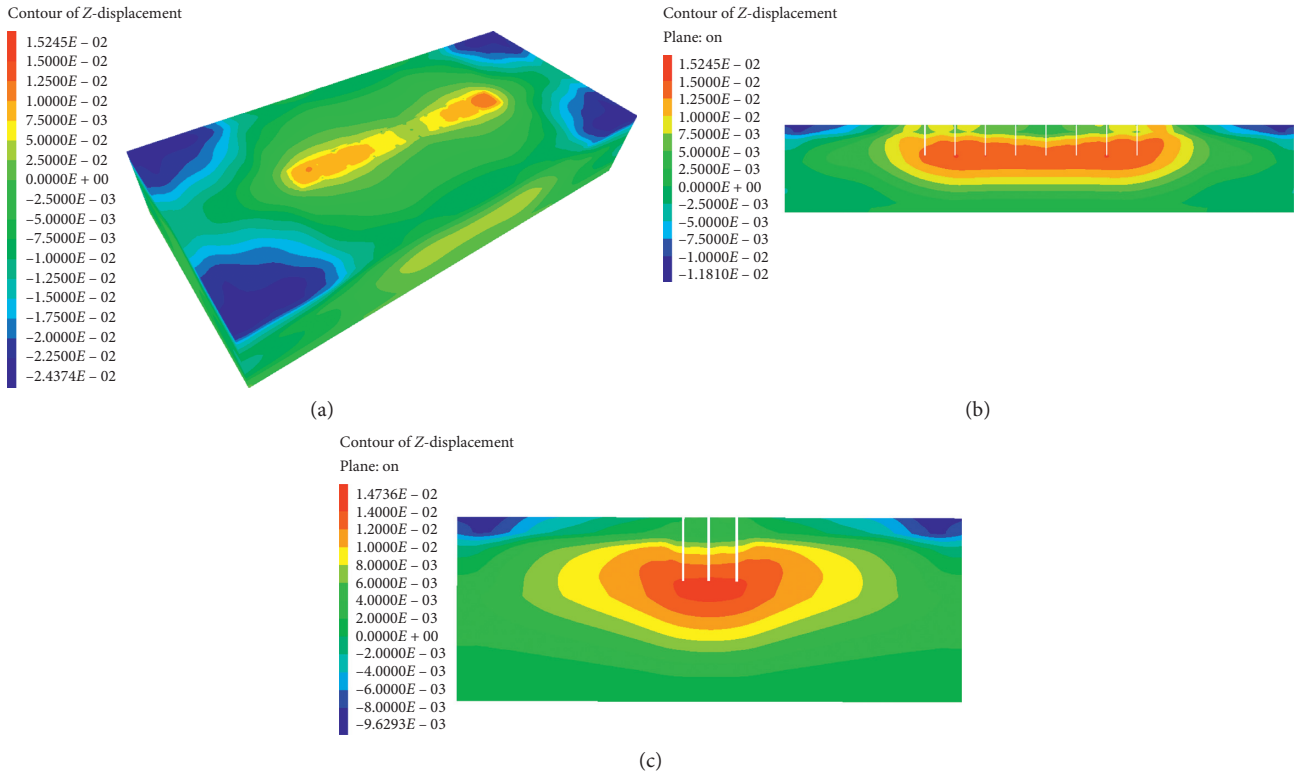

Figure 29: Group wells subsidence nephogram after the third drawdown (unit: m). (a) Three-dimensional diagram. (b) Cross section of the well midpoint. (c) Longitudinal section of the well midpoint.

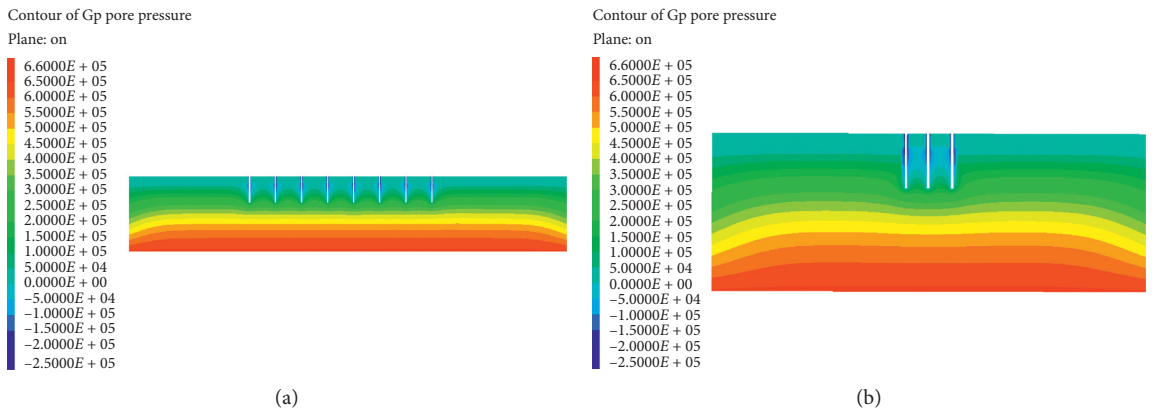

Figure 30: Group wells pore water pressure nephogram after the third drawdown (unit: Pa). (a) Cross section of the well midpoint. (b) Longitudinal section of the well midpoint.

can be quickly estimated. Therefore, the calculation results can provide effective guidance for groundwater extraction in the related foundation pit.

6. Curve Fitting for Ground Subsidence Caused by Dewatering in Foundation Pit

The variation law of ground subsidence after stabilization of groundwater drawdown is observed, and the corresponding settlement curve is proposed. The three curves obtained from field monitoring values, the calculated values under the effect of seepage force, and the numerical simulation are all consistent with each other as shown in Figure 35.

It is clearly seen from Figure 35 that the ground subsidence obtained by using the normative algorithm are conservative, and the ground subsidence obtained by numerical simulation and seepage force are close to the on-site monitoring values. Moreover, the ground subsidence calculated by using the algorithm under the action of seepage force fits the on-site monitoring values among these methods, which shows that the calculation method of the ground subsidence under the seepage force is more accurate.

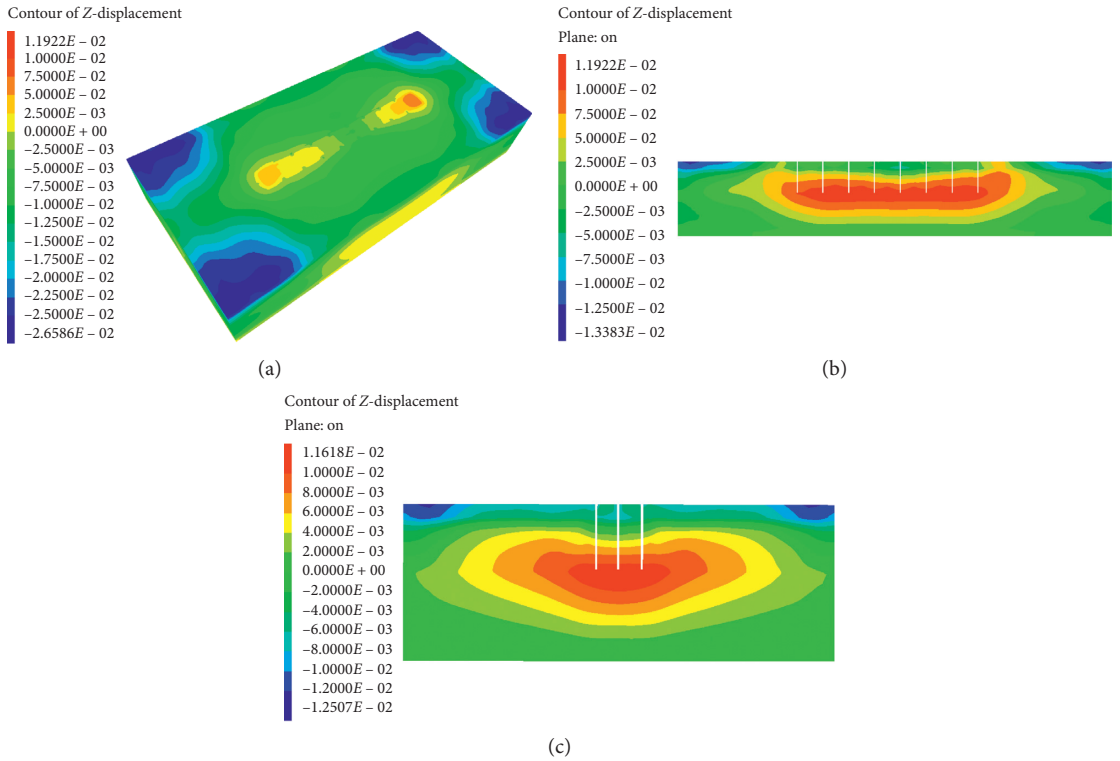

Figure 31: Group wells subsidence nephogram when the drawdown is stable (unit: m). (a) Three-dimensional diagram. (b) Cross section of the well midpoint. (c) Longitudinal section of the well midpoint.

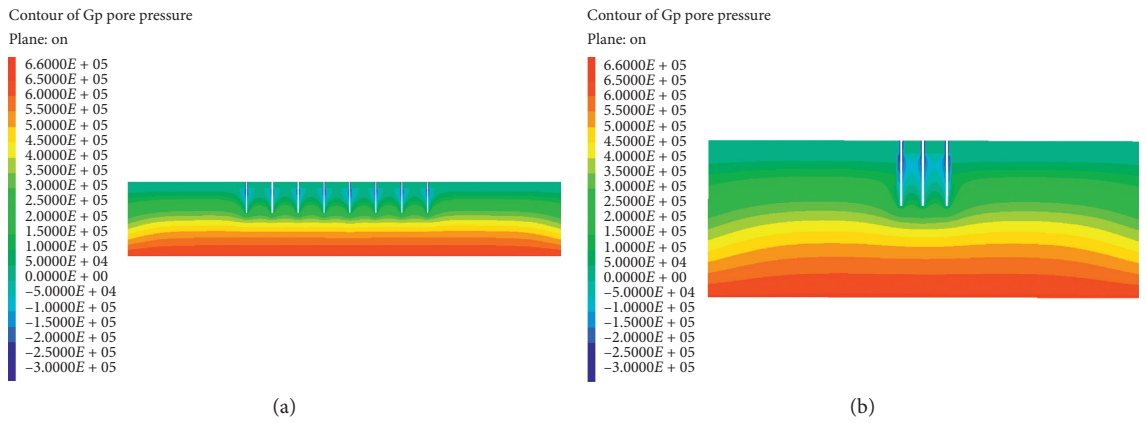

Figure 32: Group wells pore water pressure nephogram when the drawdown is stable (unit: Pa). (a) Three-dimensional diagram. (b) Cross section of the well midpoint.

The ground subsidence curve that is fitted by the theoretical calculation can be better used to simulate the variation of ground subsidence. Referring to the research results in reference [30], the ground subsidence $Z(x)$ is easily obtained as expressed below:

$$Z(x) = -be^{-(x/c)}, \quad x > 0, \tag{43}$$

where x denotes the distance from the monitoring point to the foundation pit, m; b and c indicate coefficients to be determined, respectively; and $Z(x)$ represents the ground subsidence, mm.

Substituting numerical values into equation (43), and after calculation, the ground subsidence-fitting curve is obtained as shown below:

$$Z(x) = -9.71e^{-(x/12.11)}, \quad x > 0. \tag{44}$$

Since this equation is obtained based on the actual project, it has provided specific guidance for the assessment of ground settlement due to the dewatering in foundation pit of the subway station on Chengdu metro line 6. And it can also be used to calculate ground subsidence due to similar foundation pit dewatering in sandy pebble soil strata.

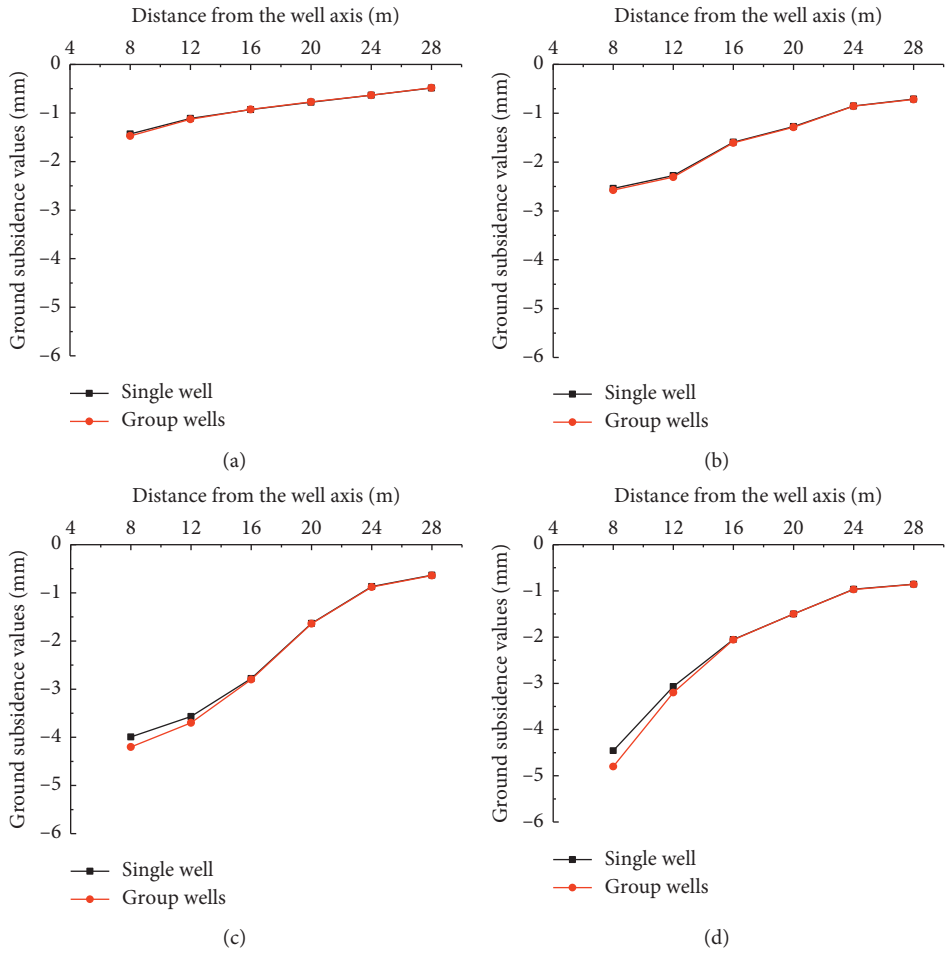

Figure 33: Comparison of ground subsidence around single well and group wells under different drawdowns. (a) Grade I drawdown. (b) Grade II drawdown. (c) Grade III drawdown. (d) Grade IV drawdown (drawdown stability).

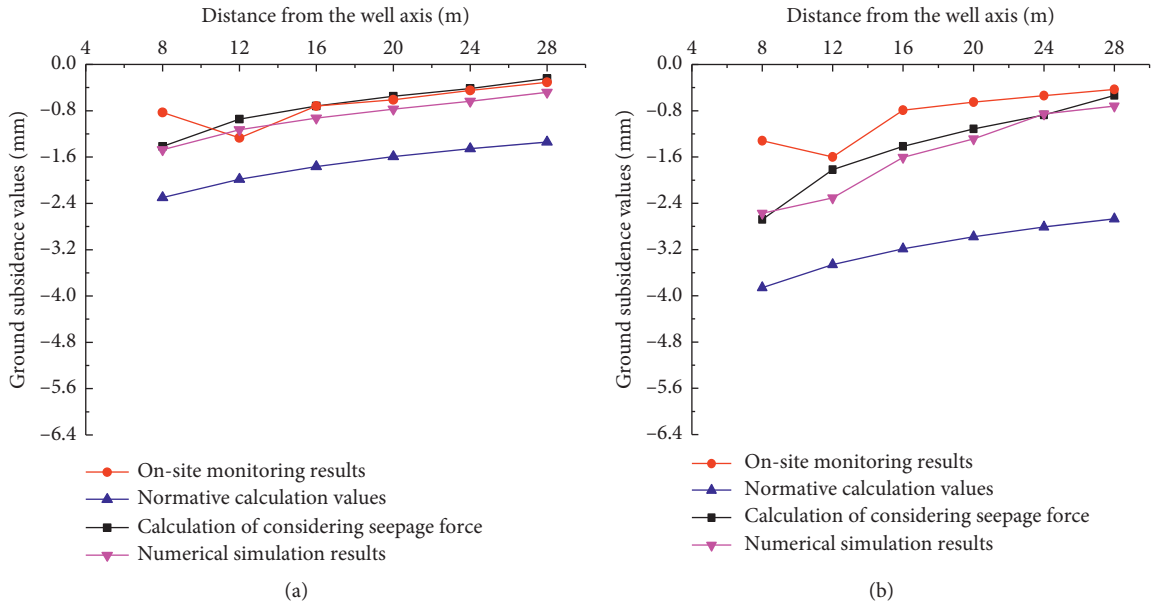

Figure 34: Continued.

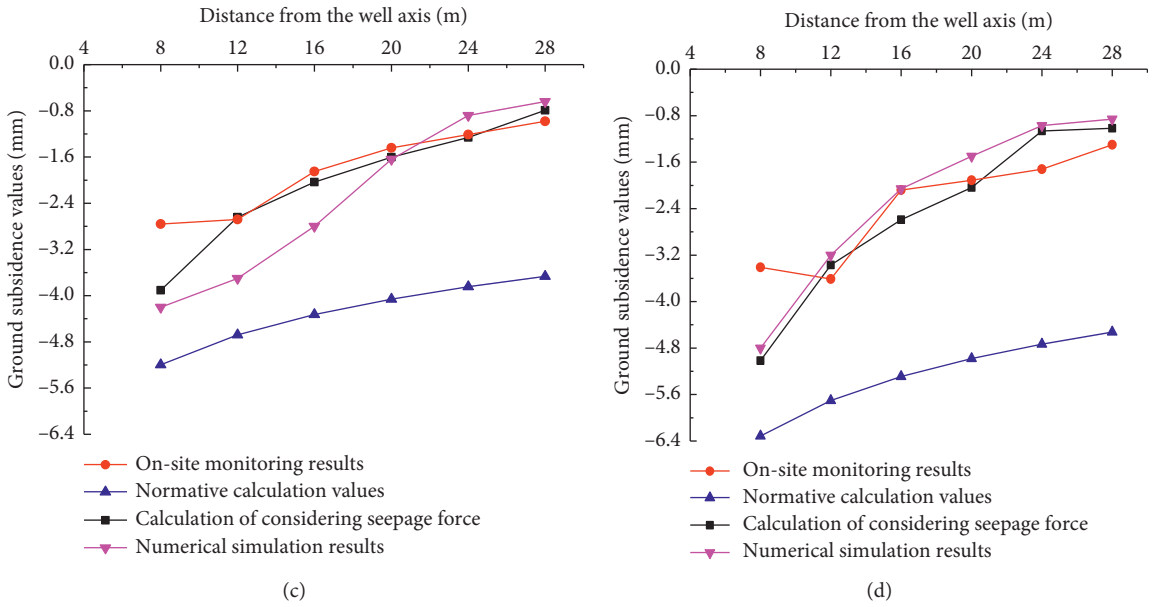

Figure 34: Comparison of settlements at different distances from well axis under different drawdowns. (a) Grade I drawdown. (b) Grade II drawdown. (c) Grade III drawdown. (d) Grade IV drawdown (drawdown becomes stable).

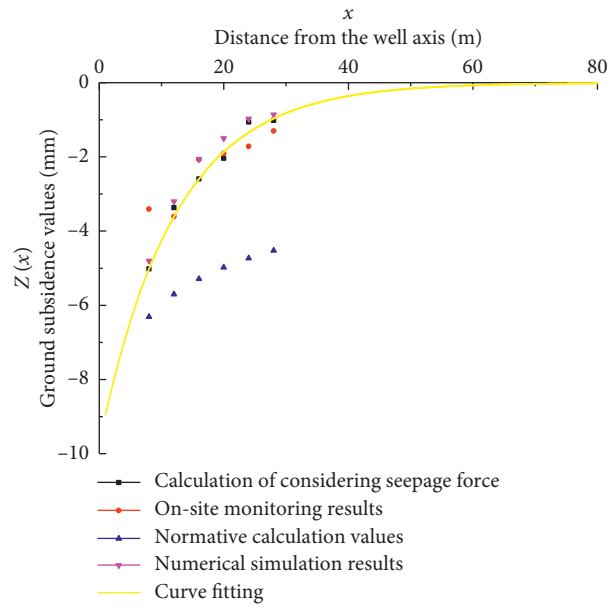

Figure 35: Curve fitting for ground subsidence around the foundation pit.

Calibration was accomplished by applying a set of hydraulic parameters, boundary conditions, and stresses that produce computer-generated simulated pressure heads that match actual field measurement within an acceptable range of error. Model calibration was performed manually (trial and error) and automatically. The model is calibrated by applying the permeability coefficient and the ground subsidence around the foundation pit under different drawdowns, as well as limiting the normal displacement and the bottom displacement of the four sidewalls and bottom of the model, while limiting the horizontal displacement of the dewatering wells. The bottom part of the filter pipe of the dewatering wells belongs to the seepage boundary. Based on the on-site monitoring, the improved settlement calculations under the action of seepage force, and the conventional algorithm proposed in the Chinese Specification, the ground subsidence around the foundation pit under different drawdowns is obtained. The comparison of ground subsidence due to different drawdowns is used to calibrate the model.

7. Conclusions

(1) According to the assumption of seepage field at the bottom of the enclosure structure in the open cut foundation pit, the influence range of the dewatering well inside open cut foundation pit and the calculation method of the water inflow are presented by using the principle of equality of water inflow inside the pit and outside the pit. The corresponding design of the foundation pit is also carried out in combination with the actual project.

(2) The dewatering funnel curve of the dewatering well in the phreatic aquifer is derived using Dupuit's assumption, and the groundwater levels at different locations under different drawdowns are obtained. Through the comparison of the results obtained from the Chinese Specification, the algorithm considering the seepage force, the numerical simulation, and the on-site monitoring of the ground settlement, the overall trend of ground settlement in these four cases is basically consistent, and the ground subsidence around the foundation pit increases with the gradual proceeding of dewatering. The farther the monitoring point is away from the well axis, the smaller the ground subsidence becomes. Moreover, the current normative calculation method recommended in the Chinese Specification is more conservative. However, the calculation method considering the action of seepage force is more accurate, and it can provide a theoretical basis for the estimation of ground subsidence caused by dewatering in the foundation pit in actual engineering.

(3) The three-dimensional fluid-solid coupling numerical simulation of the ground subsidence caused by dewatering inside the foundation pit is carried out using the finite difference method. The simulation of dewatering in the foundation pit under the single well and the group wells effect was carried out separately, and the group wells effect of the ground subsidence around the foundation pit was analyzed. The results show that the dewatering in the foundation pit will cause the upheaval of the strata inside the foundation pit and the ground subsidence outside the pit. The variation trend of ground subsidence around the foundation pit caused by the single well and group wells dewatering at each drawdowns is the same. The group wells effect on the ground subsidence after dewatering inside the foundation pit is not obvious, especially when it is far away from the foundation pit or the drawdown is not large.

(4) By fitting the ground subsidence value calculated using the algorithm considering the effect of seepage force on a metro station on Chengdu Metro Line 6, the final ground subsidence curve is obtained as shown in equation (44). The curve can be used to accurately simulate the ground settlement trend induced by dewatering inside the foundation pit in the actual project, which provides effective guidance for the similar dewatering project inside open cut foundation pit in sandy pebble stratum.

(5) A practical project in sandy pebble soil strata is taken as an example to study the ground subsidence caused by dewatering in the foundation pit in this paper. Similarly, for other geological conditions, corresponding conclusions can also be obtained using the same way in the paper.

Data Availability

All data and models employed to support the findings of this work are available from the corresponding author upon request.

Conflicts of Interest

The authors declare that they have no conflicts of interest.

Acknowledgments

The authors are grateful to the support of Research and Development Program of the 21st China Railway Construction Corporation Ltd.

References

[1] Y. Yihdego, "Evaluation of flow reduction due to hydraulic barrier engineering structure: case of urban area flood, contamination and pollution risk assessment," *Geotechnical and Geological Engineering*, vol. 34, no. 5, pp. 1643–1654, 2016.

[2] X. Zhang, X. Ou, J. Yang, and J. Fu, "Deformation response of an existing tunnel to upper excavation of foundation pit and associated dewatering," *International Journal of Geomechanics*, vol. 17, no. 4, Article ID 04016112, 2017.

[3] J. Wang, Y. Wu, X. Liu, T. Yang, H. Wang, and Y. Zhu, "Areal subsidence under pumping well–curtain interaction in subway foundation pit dewatering: conceptual model and numerical simulations," *Environmental Earth Sciences*, vol. 75, no. 3, p. 198, 2016.

[4] Y. Xu, H. Nawu, B. Z. Wang, and T. Yang, "Dewatering induced subsidenceduring excavation in a Shanghai soft deposit," *Environmental Earth Sciences*, vol. 76, no. 9, p. 351, 2017.

[5] J. Wang, X. Liu, S. Liu, Y. Zhu, W. Pan, and J. Zhou, "Physical model test of transparent soil on coupling effect of cut-off wall and pumping wells during foundation pit dewatering," *Acta Geotechnica*, vol. 14, no. 1, pp. 141–162, 2019.

[6] E. Pujades, S. De Simone, J. Carrera, E. Vázquez-Suñé, and A. Jurado, "Settlements around pumping wells: analysis of influential factors and a simple calculation procedure," *Journal of Hydrology*, vol. 548, pp. 225–236, 2017.

[7] J. Wang, B. Feng, H. Yu, T. Guo, G. Yang, and J. Tang, "Numerical study of dewatering in a large deep foundation pit," *Environmental Earth Sciences*, vol. 69, no. 3, pp. 863–872, 2013.

[8] J. Wang, X. Liu, Y. Wu et al., "Field experiment and numerical simulation of coupling non-darcy flow caused by curtain and pumping well in foundation pit dewatering," *Journal of Hydrology*, vol. 549, pp. 277–293, 2017.

[9] Y. X. Wu, H. Min Lyu, J. Han, and S. Shen, "Dewatering induced building settlement around a deep excavation in soft deposit in Tianjin, China," *Journal of Geotechnical and Geoenvironmental Engineering*, vol. 145, no. 5, Article ID 05019003, 2019.

[10] D.-d. Zhang, C.-y. Song, and L.-z. Chen, "Numerical evaluation of land subsidence induced by dewatering in deep foundation pit," *Journal of Shanghai Jiaotong University (Science)*, vol. 18, no. 3, pp. 278–283, 2013.

[11] Q. Liu, J. Liu, P. Tan, Y. Li, and Z. Lin, "Calculation of water inflow of foundation pits considering water insulation effect of retaining structures," *Tunnel Construction*, vol. 33, no. 2, pp. 142–146, 2013, in Chinese.

[12] S. J. Kollet and R. M. Maxwell, "Capturing the Influence of groundwater dynamics on land-surface processes using an integrated, distributed watershed model," *Water Resources Research*, vol. 44, 2008.

[13] Z.-j. Luo, Y.-y. Zhang, and Y.-x. Wu, "Finite element numerical simulation of three-dimensional seepage control for deep foundation pit dewatering," *Journal of Hydrodynamics*, vol. 20, no. 5, pp. 596–602, 2008.

[14] W. Dragoni, "Some considerations regarding the radius of influence of a pumping well," *Hydrogeology*, no. 3, pp. 21–26, 1998.

[15] Y. Yihdego, "Engineering and enviro-management value of radius of influence estimate from mining excavation," *Journal of Applied Water Engineering and Research*, vol. 6, no. 4, pp. 329–337, 2018.

[16] Y. Yihdego and L. Drury, "Mine dewatering and impact assessment in an arid area: case of Gulf region," *Environmental Monitoring and Assessment*, vol. 188, no. 11, 2016.

[17] Y. Yihdego and A. Paffard, "Predicting open pit mine inflow and recovery depth in the Durvuljin soum, Zavkhan province, Mongolia," *Mine Water and the Environment*, vol. 36, no. 1, pp. 114–123, 2017.

[18] JGJ 120-2012, *Technical Specification for Retaining and Protection of Building Foundation Excavations*, China Building Industry Press, Beijing, China, 2012, in Chinese.

[19] JGJ 111-2016, *Technical Code for Groundwater Control in Building and Municipal Engineering*, China Building Industry Press, Beijing, China, 2016, in Chinese.

[20] C. Hu, Z. Zhou, Y. Li, and Li Yuan, "Analysis of the ground subsidence caused by dewatering in deep foundation pit," in *Proceedings of the International Conference of the Associated Research Centers for Urban Underground Space*, Shenzen, China, November 2009.

[21] J. Bear, *Hydraulics of Groundwater*, Courier Corporation, Chelmsford, MA, USA, 2012.

[22] Y. Wu and Y. Zhu, "The simplified calculation and well-pumping test of settlement on the dewatering of foundation pits location in phreatic aquifer," *Journal of Civil, Architectural and Environmental Engineering*, vol. 37, no. S2, pp. 168–177, 2015, in Chinese.

[23] Q. Yang and B. Zhao, "Experimental and theoretical study on the surface subsidence by dewatering of foundation pit in phreatic aquifer," *Chinese Journal of Rock Mechanics and Engineering*, vol. 37, no. 6, pp. 1506–1519, 2018, in Chinese.

[24] S.-L. Shen and Y.-S. Xu, "Numerical evaluation of land subsidence induced by groundwater pumping in Shanghai," *Canadian Geotechnical Journal*, vol. 48, no. 9, pp. 1378–1392, 2011.

[25] D. D. Zhang, "Coupled numerical simulation research on dewatering and land subsidence in deep foundation pit," *Applied Mechanics and Materials*, vol. 275–277, pp. 1549–1552, 2013.

[26] N. Zhou, P. A. Vermeer, R. Lou, Y. Tang, and S. Jiang, "Numerical simulation of deep foundation pit dewatering and optimization of controlling land subsidence," *Engineering Geology*, vol. 114, no. 3-4, pp. 251–260, 2010.

[27] Y.-Q. Zhang, J.-H. Wang, J.-J. Chen, and M.-G. Li, "Numerical study on the responses of groundwater and strata to pumping and recharge in a deep confined aquifer," *Journal of Hydrology*, vol. 548, pp. 342–352, 2017.

[28] J. Wang, B. Feng, Y. Liu et al., "Controlling subsidence caused by de-watering in a deep foundation pit," *Bulletin of Engineering Geology and the Environment*, vol. 71, no. 3, pp. 545–555, 2012.

[29] M. N. Houhou, F. Emeriault, and A. Belounar, "Three-dimensional numerical back-analysis of a monitored deep excavation retained by strutted diaphragm walls," *Tunnelling and Underground Space Technology*, vol. 83, pp. 153–164, 2019.

[30] F. Li and G. Chen, "Study of ground surface settlement of foundation pit with suspended waterproof curtain in Yangtze river flood plain," *Tunnel Construction*, vol. 38, no. 1, pp. 33–40, 2018, in Chinese.

[31] X. Zhou, H. Hu, B. Jiang, Y. Zhou, and Y. Zhu, "Numerical analysis on stability of express railway tunnel portal," *Structural Engineering and Mechanics*, vol. 57, no. 1, pp. 1–20, 2016.